



Abundance, distribution, and ecological/environmental risks of critical rare earth elements (REE) in phosphate ore, soil, tailings, and sediments: application of spectroscopic fingerprinting

Faten Khelifi¹ · Sadia Batool² · Rabah Kechiched³ · Elio Padoan¹ · Kaouther Ncibi⁴ · Younes Hamed⁴

Received: 1 September 2023 / Accepted: 29 February 2024
© The Author(s) 2024

Abstract

Purposes This research focuses on the characterization of phosphate ore, its solid effluents, and nearby contaminated soils in the southwest Tunisia (Gafsa-Metlaoui Basin). It aims also at evaluating the vertical distribution and abundance of critical rare earth elements (REE) in the different materials and their ecological and environmental risks.

Materials and methods The sampled materials went through physical, chemical, and mineralogical characterization which involved XRF, XPS, XRD, and ICP-MS analyses. The REE anomalies and the environmental and ecological indices were calculated.

Results and discussions Results show relatively high concentrations of nine rare REEs, following the sequence La > Ce > Nd > Y > Gd > Eu > Sm > Yb > Tb and trace metal elements (TME) such as Cd, Cr, Mn, Zn, Co, Fe, Sr, Cu, Ni, Pb, Ba that surpass, in some cases, international standards. The vertical distribution of the studied elements within a sediment, tailings, and soil profiles (beyond 20 cm of depth) indicates their likely in-depth migration. TME- and REE-bearing phosphate samples reflect mostly oxic conditions in the southern area with high positive Eu anomalies signifying possible mixing of sources. The environmental assessment indicate no contamination and a moderate enrichment of REEs, except for Eu, which displays significant contamination and extreme enrichment. Whereas, a deficiency of Y has been detected in most of the studied samples except for sludge sample which was also found significantly enriched with REE.

Conclusions There are fundamental similarities between the different studied samples with high carbonate mineral concentrations. Statistical analysis confirmed the spectroscopic fingerprints demonstrating that the different materials share a similar composition. All of these similarities are most likely linked to the impact of mining activities on sediments and soils. Overall, our findings highlight the global effect of ore processing in determining the geochemical and the mineralogical characteristics of the surrounding environments of mines.

Keywords Mining district · Rare earth elements (REE) · Geochemical characterization · XPS · Mineralogical composition · Paleoenvironment · Ecological risk · Southern Tunisia

1 Introduction

Mineral extraction and processing produce crushed and milled wastes which, when weathered, pose a risk to the environment. In the absence of waste management legislations, these wastes can turn into a significant hazard to

the environment (Avila et al. 2008; Khelifaoui et al. 2020; Padoan et al. 2020).

The growing demand for commercial phosphate, especially for the agricultural sector, has led to a thriving phosphate mining industry and a subsequent increase of waste production. Millions of tons of various types of wastes (e.g., tailings, sludges) per year (Eskanlou and Huang 2021) are currently generated, with a ratio of 1 to 12 tons per one ton of phosphate (Taha et al. 2021). These wastes, in turn, contain large amounts of trace metals (e.g., Cd, Cr, Zn, Pb), rare earth elements (REE), and radioactive elements that could,

Responsible editor: Milica Kašanin-Grubin

Extended author information available on the last page of the article

potentially, leach from their bearing rock to pollute soils, plants, and groundwater (Al-Hawaiti et al. 2016). Furthermore, potentially toxic trace element (PTE) leaching from P-bearing deposits is a common issue that comes entangled with several socio-economic problems and physiological and environmental risks (Hamed et al. 2022). To map these risks, extensive mineralogical and geochemical analyses could serve for assessing and quantifying the environmental damages caused by the mining industry, and thus, guide the site remediation and land reclamation strategies.

For decades, the Gafsa mining basin has been one of the most polluted regions in Tunisia in terms of soil, stream sediments, and air. The diffused pollution is mainly associated with the operational phosphate ore extraction and processing activities. Sampled stream sediments, tailings, and soil were proven to be contaminated by potentially toxic elements (PTE), such as Cd, Cr, Pb, and Zn, and the site was globally classified as heavily contaminated (Khelifi et al. 2021). The PTE concentrations, particularly within stream sediments, and tailings exceeded by far international thresholds, namely, Non-Polluted Sediments standards (NPS) (Khelifi et al. 2020a, b). Meanwhile, the occurrence of REEs and trace metals in Tunisian phosphates, stream sediments, sludge, and tailings carried out in Gafsa-Metlaoui mining basin was thoroughly studied by Galfati et al. (2014), revealing that solid effluents of phosphate mines are relatively depleted in REE compared to the washed ore ($\sum \text{REE} = 182 \text{ ppm}$). Furthermore, REE variation within sedimentary phosphates and the geologic processes which govern them are still a matter of controversy among researchers (Emsboet al. 2015). Ferhaoui et al. (2022) indicated that REE occurrence and distribution in Northern African P-deposits are mostly controlled by the depositional environments rather than secular variations during geological ages. However, the study has not further examined the geochemical process controlling their distribution in phosphate effluents or their potential environmental risks.

Beyond PTE contamination, research projects which were conducted on the neighboring, yet similar, basins of Algerian Paleocene-Eocene phosphates (Boumaza et al. 2021; Kechiched et al. 2020; Ferhaoui et al. 2022) revealed that REE were found in relatively high amounts. Moreover, in the study of Kechiched et al. (2018), total REE concentrations were found to be significant ($\sum \text{REE} > 1000 \text{ mg.kg}^{-1}$) within glauconitic particles from the Algerian phosphates, whereas lower average concentrations ($\sum \text{REE} = 322 \text{ mg.kg}^{-1}$) were recorded in the Gafsa basin (Garnit et al. 2017). However, the REE concentrations in phosphates rock (PR) of Gafsa basin are considered REE-poor PR compared to other Tunisian basins which elucidated values exceeding 1700 ppm. Thus, Tunisian PR is considered the most REE-enriched rock compared to other deposits around the world such as the Algerian, Chinese, American, or Moroccan phosphates

(El Zrelli et al. 2021). Recently, the study of Buccione et al. (2021) focused on comparing North African REE-bearing phosphate deposits, indicated that REEs in the Algerian-Tunisian basin share common geochemical patterns, while Moroccan ones appear significantly different in terms of REE contents and paleo-environment characteristics. Furthermore, these deposits were proven to be a pool of possibly extractable critical REE which, in their turn, could be used and applied in modern industries (e.g., automotive, electronics). Actually, REEs are of paramount importance due to their multipurpose industrial uses (e.g., fabrication of magnets, glass, ceramics, batteries; Yang et al. 2024). In the near future, REE increasing demand will result in possible shortages of their conventional sources (xenotime, monazite, bastnäsite), making it critical to identify low-cost and efficient alternatives (e.g., extraction from E-wastes and mine wastes). Indeed, phosphates and their wastes could be considered significant REE-bearing sedimentary minerals capable of serving as an alternate supply of REE (Ounis et al. 2008; Emsbo et al. 2015; Buccione et al. 2021).

In this context, the present study uses spectroscopic fingerprinting to highlight the relationship between geochemical and mineralogical composition of sediments, soil, phosphate ore, and its wastes, as well as between the studied elements, identifying their potential common sources while reconstructing the paleo-depositional environment and redox conditions. It also aims at providing a preliminary insight into the abundance of some REE within stream sediments and the soil that are mainly affected by mine liquid wastes and solid tailings of the phosphate ore. Additionally, the study attempts to assess the potential environmental and ecological risks associated with critical REE in the different sampled materials which, up to the present date, have not been discussed in previous studies.

2 Materials and methods

2.1 Mining activities in the study area

The study area is located in southwestern Tunisia close to the Algerian borders (Fig. 1). The basin of Gafsa-Metlaoui is characterized by its semi-arid climate, with its typical features of high temperatures during summers occasionally exceeding 45 °C, high evapotranspiration (1680 mm year⁻¹), low precipitation rates (average of ~183 mm in 2018), and sparse vegetation cover. The city is mostly known for the industrial activities of phosphate extraction and processing. Due to the peculiarity of the area (e.g., climatic, geographic) and the absence of alternative sectors (e.g., agriculture, tourism, services), the region depends solely on the industrial activities of phosphates (Hamed et al. 2022).

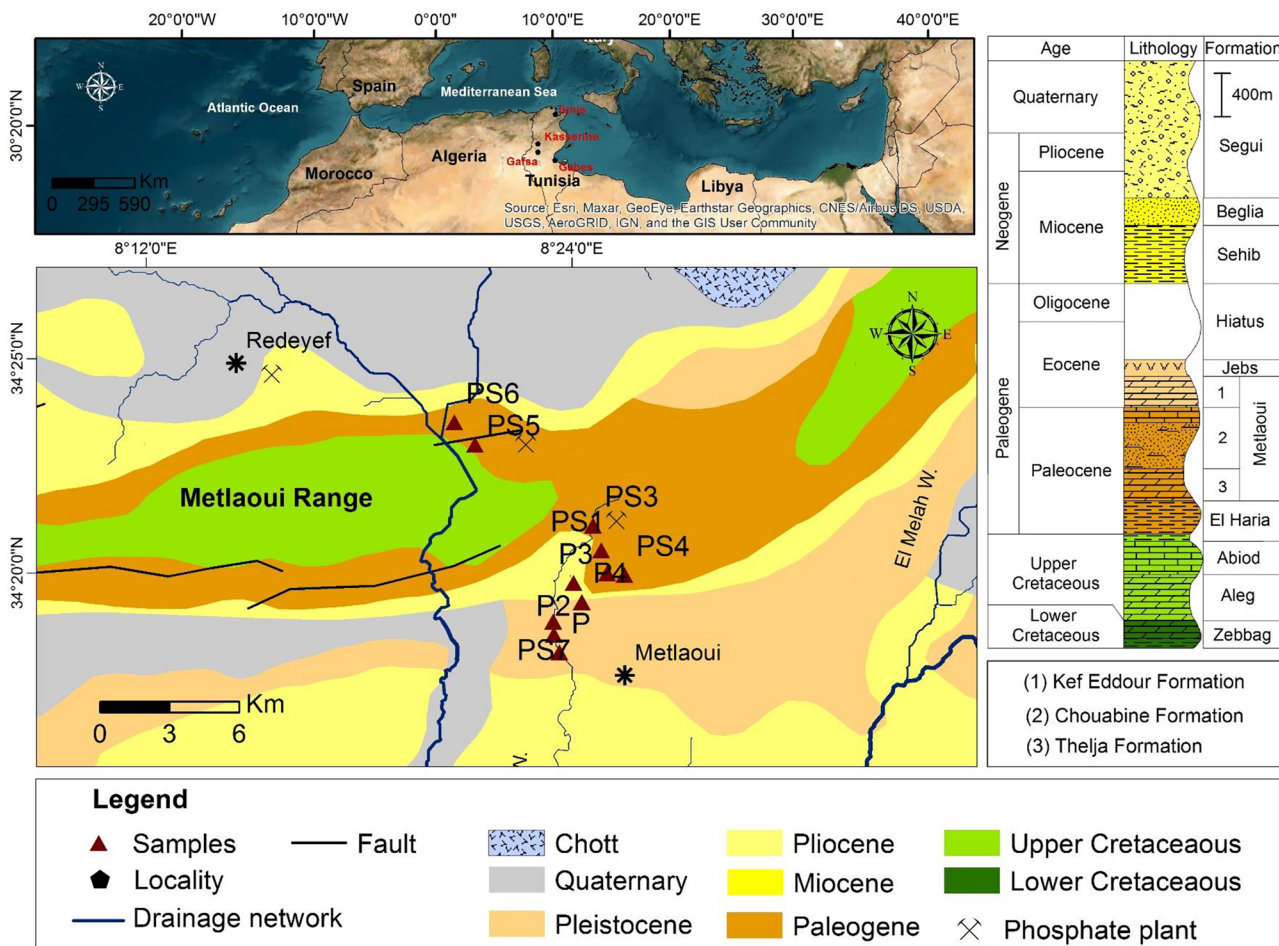


Fig. 1 Sampling location on the geologic map (from Bel Haj Ali et al. 1987) and simplified lithostratigraphic column of the study area (after Hamed 2013)

Actually, the phosphate industry plays a pivotal role not only on regional scale but also on national and international levels, boosting for that matter the economy, the export, and the foreign currency provision. Several deposits of phosphates in Tunisia were deposited during Paleocene-Eocene age around the city of Kasserine formerly called “Kasserine Island.” The most exploited mines are those of Gafsa basin, which contain the largest reserves. Typically, the ore is washed and processed within the mining area. The extracted materials undergo exhaustive multi-step processing (e.g., crushing, sieving, washing, flotation) to obtain a P₂O₅-rich fraction, discarding the accessory matrix, which is considered a “minefield” of potentially toxic trace elements.

The enrichment process generates various kinds of by-products which are disposed either in the water streams (in form of sludge and wastewater) or on the ground in the vicinity of urban sites (in form of solid wastes piles). The dumping sites are almost entirely uncontrolled sites where the wastes are poorly managed. Simultaneously, fine particles

from the solid waste piles and the dredged/dry sludge are eventually suspended in the atmosphere.

2.2 Geological settings

Previous studies (e.g., Kocsis et al. 2014) attributed the phosphatic deposits of central and southwest Tunisia to the tectonic events of Late Cretaceous which affected the paleogeographic scene during Paleocene and Eocene. Thus, the shallow marine borders of the prehistoric ocean “Tethys,” interrupted by the “Island of Kasserine” formed an adequate location for the circulation of upwelling currents, the accumulation of organic matter, and the deposition of sedimentary phosphates.

The main series of Metlaoui Group deposited during late Paleocene-Early Eocene. The Metlaoui Group was first defined at its typical location of Thelja area. Furthermore, a cross-section of the area showed three units formed of i) evaporitic deposits with clays, fossiliferous dolomites, and gypsum of Thelja formation (named after its typical

location of Thelja area); ii) intercalation of gray marls with phosphatic limestones, limestones, phosphate levels with lamellibranches of Chouabine formation; and iii) deposits of phosphatic conglomerates to the bottom, and a thick calcareous layer to the top of Kef Eddour formation in its typical emerging area of Kef Eddour sector KD (ElAyachi et al. 2016). This sector contains one phosphate processing factory (plant V), while the other two factories (plants III and IV) (within the city) belong to Kef Schfaïr sector KS (Fig. 1).

2.3 Sampling and instruments

Samples comprised two sediment profiles, namely, P (20 subsamples) and P2 (22 subsamples), which were collected from Sebseb wadi, one tailing profile P3 (20 subsamples) and surface tailing PS4 sampled from a tailing pile stacked in the urban area, five phosphate rock (PS1, PS2, and PS3 referred as PKS; PS5 and PS6 referred as PKD) were gathered from Kef Schfaïr sector PKS and Kef Eddour Sector KDS and one sludge sample (PS7) sampled from the plant discarded wastes. The samples (profiles) were divided into 2-cm-thick sub-samples, counted, sorted, and only 19 samples were chosen to be further studied. The main criterion for sample selection is their position within the vertical profiles. Thus, one sample of the top (2 cm), middle (20–22 cm), and the bottom (40–44 cm) of each profile was chosen to evaluate the possible effect of depth over the different samples. Samples of sludge and phosphates are representative samples of open-cast active mines. Meanwhile vertical profile distribution that contains all obtained data of the studied elements was evaluated (see Section 3).

Overall, all the samples underwent sieving (2 mm), oven drying (105 °C, overnight), milling, chemical characterization (pH, electrical conductivity (EC), total organic carbon (TOC)), and acid digestion (HNO_3 , HCl , and HClO_4), and analyzed for metal contents and REEs. Whereas bulk samples were saved for “non-destructive” analysis. Furthermore, pH and EC were determined in 1/2.5 soil/water ratio. Meanwhile, TOC was calculated using the formula suggested by Nelson and Sommers (1982) considering TOC as 58% of OM while this later was determined using the weight loss on ignition method.

Generally, methods such as field observation, X-ray diffraction (XRD), and scanning electron microscopy (SEM) are more commonly applied as global mineralogical analysis tools, while in-depth analysis is rarely conducted by the means of methods such as X-ray photoelectron spectroscopy (XPS).

For the present study, the collected samples were subjected to different geochemical analyses, including inductively coupled plasma mass spectrometry (ICP-MS), X-ray fluorescence (XRF), and XPS analysis. XPS technique is

commonly applied to determine the elemental composition, chemical state, and binding energy of material components in surface and interfaces (Greczynski and Hultman 2020).

Similar to the study of Eusden et al. (2002), XPS analysis was applied to identify and quantify possible chemical phases of carbon, nitrogen, oxygen, fluoride, sulfur, and phosphorus. XPS was used on 19 samples with Al $K\alpha$ (1486.6 eV) source gun at 150 W with a step size of 0.05 eV (ESCALAB 250Xi, Thermo VG scientific). Binding energies values were calibrated with the C1s peak of carbon at 284.80 eV. As for data interpretation, the signals were deconvoluted using XPSPeak 41 and the peaks were identified using the Perkin-Elmer handbook for XPS analysis (Moulder et al. 1992).

XRD analysis was performed using a TTR3 diffractometer with $\text{CuK}\alpha$ radiation ($K\text{-}\alpha_1 = 1.54 \text{ \AA}$). Samples were ground to powder and scanned from 10 to 70° 2θ with a step size of 0.020°. The software X'pert highscore (2019, PANalytical) was used for mineral identification, while graphs were reproduced using Origin 9.1 (OriginLab Corp, MA, USA).

Oxides including major elements were determined in the sampled materials (sediment cores, soil, tailings, and phosphate ore) by the means of XRF (XRF-1800, Shimadzu-Japan) using rhodium X-ray tube target with a power of 4 KVA and a detection limit of 0.5 ppm. REE and trace metal elements (TME) were analyzed by ICP-MS (Agilent 7500cx, Agilent Technologies, Inc, CA, USA). Accuracy and quality assurance were checked using pre-prepared standards of known concentrations. The certified reference material (CRM-GBW07406), approved by General Administration of Quality Supervision (PRC) and provided by National Center for Standard Materials of China, was included in the analysis and obtained results were within $\pm 5\%$ of certified materials.

For data interpretation, such as REE normalization and anomaly calculations, statistical analysis, and ecological/environmental ecological risk assessments, only average values for each set of samples were considered.

2.4 REE anomalies and statistical analysis

REE in phosphate deposits are mostly used as tracers of paleoenvironments, paleogenesis, paleo-productivity, and paleoredox conditions (Shields and Stille 2001; Xin et al. 2016; Garnit et al. 2017; Zarasvandi et al. 2021; Creac'h et al. 2023). Mostly, Ce and Eu anomalies are calculated for phosphate samples using the following formulas $Ce_{an} = \log Ce/Ce^*$, where $Ce/Ce^* = 3Ce_N/2La_N + Nd_N$ (Wright et al. 1987), and $Eu_{an} = Eu/Eu^*$, where Eu/Eu^* is expressed as $Eu_N/(Sm_N + Gd_N)^{0.5}$. While N refers the Post-Archean Australian Shale (PAAS) normalized values. Along with Ce and Eu anomalies, La anomaly and the characteristic parameters

of REE, namely, La_N/Yb_N , La_N/Sm_N , and Gd_N/Yb_N , were calculated (Wu et al. 2018; Li et al. 2022).

Many authors (e.g., Pawlowsky-Glahn et al. 2015; Barceló-Vidal and Martín-Fernández 2016) have raised substantial problems in using raw data to compute Pearson correlations leading to inaccurate results and generating misleading data due to “closure” effect. Therefore, in preparation for the application of statistical tests such as principal component analysis (PCA) and hierarchical cluster analysis (HCA), the geochemical data were converted to ppm. The data were transformed using centered log-ratio (clr) transformation following the Euclidean geometry in real space, which was applied in many previous studies (e.g., Aitchison 1982; Reimann et al. 2008; Blake et al. 2016). It is worth mentioning that for CoDa techniques, the absence of data in a compositional dataset can prevent the conversion of raw data to clr-data (Palarea-Albaladejo et al. 2014; Buccianti et al. 2014); thus, in the present data we have excluded Pb, Co, and Nd due to missing values. The transformation of data into clr-ratios was computed using CoDa Pack software (Comas-Cufí and Thió-Henestrosa 2011). Prior to PCA, Pearson correlations on clr-data were used to interpret elemental inter-relationships between the variables. It was used also for calculation of the distances between the variables/individual and Pearson correlations using an average-linkage clustering method (for agglomerative clustering) were used for conducting HCA. The XLSTAT software (Addinsoft 2021) was used for PCA and HCA calculations.

2.5 Environmental and ecological assessments

Geoaccumulation index was calculated using the formula $I_{\text{geo}} = \text{Log}_2 (C_E/1.5 C_B)$. It involves seven classes of contamination: less than zero absent, 0–1 absent to moderate, 1–2 moderate, 2–3 moderate to heavy, 3–4 heavy, 4–5 heavy to extreme, and above 5 extreme contamination levels (Muller 1969).

Potential ecological risk index (RI) implemented earlier by Hakanson (1980) and applied recently by El Zrelli et al. (2021) was calculated as the sum of the subsequent index of each element which is expressed as $RI = \sum E_r^i$ with $E_r^i = \frac{T_r^i \times C_m^i}{C_n^i}$, where T_r^i is the toxic level coefficient, and C_m^i and C_n^i are the concentrations of the specific element i of the sample and of the background value respectively. In other words, the ecological risk is a function of the contamination factor expressed as the ratio of the element's concentration and its reference value. The risk would be considered very high only if $RI \geq 600$, considerable if $300 \leq RI < 600$, moderate if $150 \leq RI < 300$, and low if $RI < 150$. Due to the lack of local standards, we referred to Post-Archean Australian Shale PAAS and Upper Continental Crust UCC background values.

3 Results and discussions

3.1 Geochemical characterization

All samples were neutral to slightly alkaline, with pHs between 7 and 8. The neutral to alkaline pH is mainly induced by the relatively high carbonate content which is, in its turn, inherited from the nature of the bedrock materials. Total organic carbon (TOC) yielded values that are mostly less than 10% with a moderate organic matter content that is mainly controlled by pedogenic processes and influenced by the ore processing activities.

Generally, TME (Cd, Cr, Mn, Zn Co, Fe, Sr, Cu, Ni, Pb, Ba) concentrations showed higher amounts of Fe, Zn, and Sr on the expense of other elements (Table 1). In the meantime, considering vertical distribution, all of them showed a tendency to increase toward deeper layers particularly for the sediment profile P2 (Khelifi et al. 2021). Accordingly, higher amounts of TME were recorded among the phosphate samples. To a lesser extent, trace metals within solid effluents of Sebseb stream, for the most part in deep sampled sediments (sample SB1), were of high contents. Considering its high toxicity and low threshold, Cd, in particular, was found in significant concentration in phosphates, tailings, and deep stream sediments. Such observation leads to the fact that a great share of potentially harmful elements remains within the mine wastes.

Overall, regardless of the nature of the studied materials, many factors could interfere with the geochemical distribution of these trace elements in a certain material such as the chemical characteristics of the element itself (e.g., ionic radii, valence) that allow its ability to substitute a major element. They are also highly governed by the bearing matrix, its mineralogical composition, as well as grain size distribution (finer fraction is a typical trace element-rich fraction).

3.2 Mineralogy

The XRD diffractograms of the top samples (0–2 cm) as well as the in-depth samples (40 cm) of the sediment profiles (P, P2) shown in Fig. 2 indicates that apatite was the most abundant mineral in the studied samples. Samples of profile P2 of the 2 and 40 cm depth showed similar patterns with higher intensity peaks for deeper sediments.

The mineralogical composition of steam sediments and phosphate samples was represented mainly by carbonate-fluorapatite (CFA, $\text{Ca}_5\text{F}(\text{PO}_4)_3$) and apatite (Fe bearing, Mn bearing). At a lesser extent, minerals such as hiortdahlite II ($\text{Ca Na}_4\text{Ca}_8\text{Zr}_2(\text{Y,Zr,Na})_2(\text{Si}_2\text{O}_7)_4(\text{O}_3\text{F}_5)$) and peroskovite Ba_2ANbO_6 ($A = \text{Tb,Gd}$) were found. It has been

Table 1 Results of major and trace elements of sampled materials of sediments profiles (P, P2) of Sebebeb stream, mine tailings (P3, PS4), soil (P4) phosphate (PKD, PKS), and sludge (PS7) samples

Unit	Sediments														Phosphates						Sludge Tailings						soil							
	P2														PKS						PKD						PS_04				P4			
	SB_22		SB_11		SB_1		SC_8		SC_4		SC_1		PS_01		PS_02		PS_03		PS_05		PS_06		P3_S1		P3_S10		P3_S20		P4_S1		P4_S10		P4_S20	
	0-2	18-12	42-44	0-5	15-20	35-40	7.5	7.6	7.5	7.7	7.6	7.7	7.5	7.5	7.5	7.5	7.5	7.5	7.6	7.6	7.5	7.6	8.00	7.47	7.41	7.6	7.55	7.66	7.84	7.90				
pH	7.5	7.6	7.5	7.5	7.7	7.6	7.7	7.5	7.7	7.6	7.7	7.5	7.5	7.5	7.5	7.5	7.5	7.5	7.5	7.6	8.00	7.47	7.41	7.6	7.55	7.66	7.84	7.90						
EC	4.0	3.1	5.0	3.7	1.3	2.1	3.0	2.8	2.5	3.0	2.8	3.0	2.8	2.5	3.0	2.8	2.5	3.0	2.6	6.73	2.97	3.22	2.92	5.66	3.48	2.65	2.55							
TOC	7.8	5.8	8.6	8.2	13.4	9.3	10.9	5.2	6.6	6.8	5.5	9.92	7.75	7.00	6.47	7.11	8.11	5.89	8.18															
CaO	27.1	35.0	33.5	27.1	32.4	42.4	29.6	42.3	45.9	38.8	39.7	23.49	34.87	25.45	24.80	43.37	29.76	29.12	35.14															
CO ₂	17.0	18.1	20.3	20.2	29.4	34.6	18.4	17.0	15.2	21.9	14.3	16.44	15.81	17.29	21.19	18.91	14.59	15.61	12.21															
SiO ₂	29.3	18.6	17.8	26.9	21.2	13.8	24.0	8.8	5.4	8.4	14.2	34.23	19.02	33.88	32.91	4.92	18.39	28.50	8.60															
P ₂ O ₅	12.0	16.5	16.5	12.2	10.5	3.1	16.0	23.2	25.2	22.1	20.5	9.89	17.43	6.05	2.86	25.03	1.44	13.75	0.89															
SO ₃	4.0	3.7	4.0	3.7	1.7	1.7	3.1	3.8	4.0	3.9	4.7	4.32	5.23	5.73	7.85	3.98	28.90	3.94	39.06															
Al ₂ O ₃	4.7	3.3	3.2	4.2	1.5	1.1	3.8	1.4	0.9	1.6	2.5	5.38	3.26	4.94	3.44	0.82	2.75	3.96	1.72															
MgO	2.4	1.7	1.6	2.0	1.1	1.9	1.9	1.0	0.7	0.8	1.5	2.40	1.70	2.73	4.18	0.75	1.54	2.14	0.93															
Fe ₂ O ₃	1.3	0.8	0.9	1.3	0.6	0.4	1.2	0.4	0.3	0.4	0.8	1.87	1.17	2.08	1.32	0.37	1.23	1.43	0.72															
Na ₂ O	0.6	0.8	0.8	0.7	0.5	0.2	0.7	1.0	1.2	1.0	0.8	0.63	0.66	0.67	0.22	1.22	0.22	0.53	0.10															
K ₂ O	0.6	0.70	0.4	0.6	0.2	0.1	0.3	0.1	0.1	0.2	0.2	0.78	0.31	0.52	0.85	0.15	0.61	0.48	0.29															
Cd	0.5*	0.4*	104*	0.1	0.2	0.2	0.2	0.1	0.3	48.8	65.2	69.3	8.69	4.32	nd	1.67	52.6	0.79	9.12	2.46														
Co	0.1	1.5	6.34	0.0	0.8	0.3	0.0	0.8	4.5	4.5	1.8	0.18	0.04	nd	nd	39.1	nd	nd	nd															
Cr	2*	5.7*	1230*	1.1	1.3	0.9	1.6	1.0	1140	1359	1029	53.6	31.85	nd	20.63	1145	7.56	1031	148															
Cu	3.9	2.8	54.4	4.4	4.0	3.5	6.2	6.4	52.7	61.7	63.5	8.44	10.93	nd	nd	65.20	nd	nd	nd															
Fe	21	35.8	38318	11.7	6.5	8.7	5.4	0.3	15514	28405	15426	2127	1070	nd	736	62981	901.13	47456	28331															
Mn	0.1*	0.2*	263*	0.1	0.1	0.1	0.1	0.0	114	157	87	9.61	5.7	nd	4.42	1027	6.98	998	351															
Ni	2.1	0.4	111	1.2	nd	0.7	0.4	0.2	102	134	128	9.01	4.4	nd	3.3	216	0.03	55.4	38.4															
Pb	2.3	6.9	0.70	3.4	4.7	2.5	nd	nd	4.2	nd	nd	1.92	4.7	nd	nd	nd	nd	nd	nd															
Sr	1.9	0.5	822	0.4	0.4	0.1	0.5	0.0	2072	2244	1847	2.27	12.6	nd	8.6	836	4.60	1069	992															
Ba	1.2	1.4	16	0.9	1.0	1.3	0.8	1.2	1.0	29.5	17.6	31.2	24.6	6.54	1.2	0.88	1.25	9.99	6.13															
Zn	18.4*	47.3*	2840*	10.8	6.96	5.3	13.4	15.8	2108	2365	3340	258	239	nd	95	1799	nd	411	257															

nd non-determined

*Values from Khelifi et al. (2021)

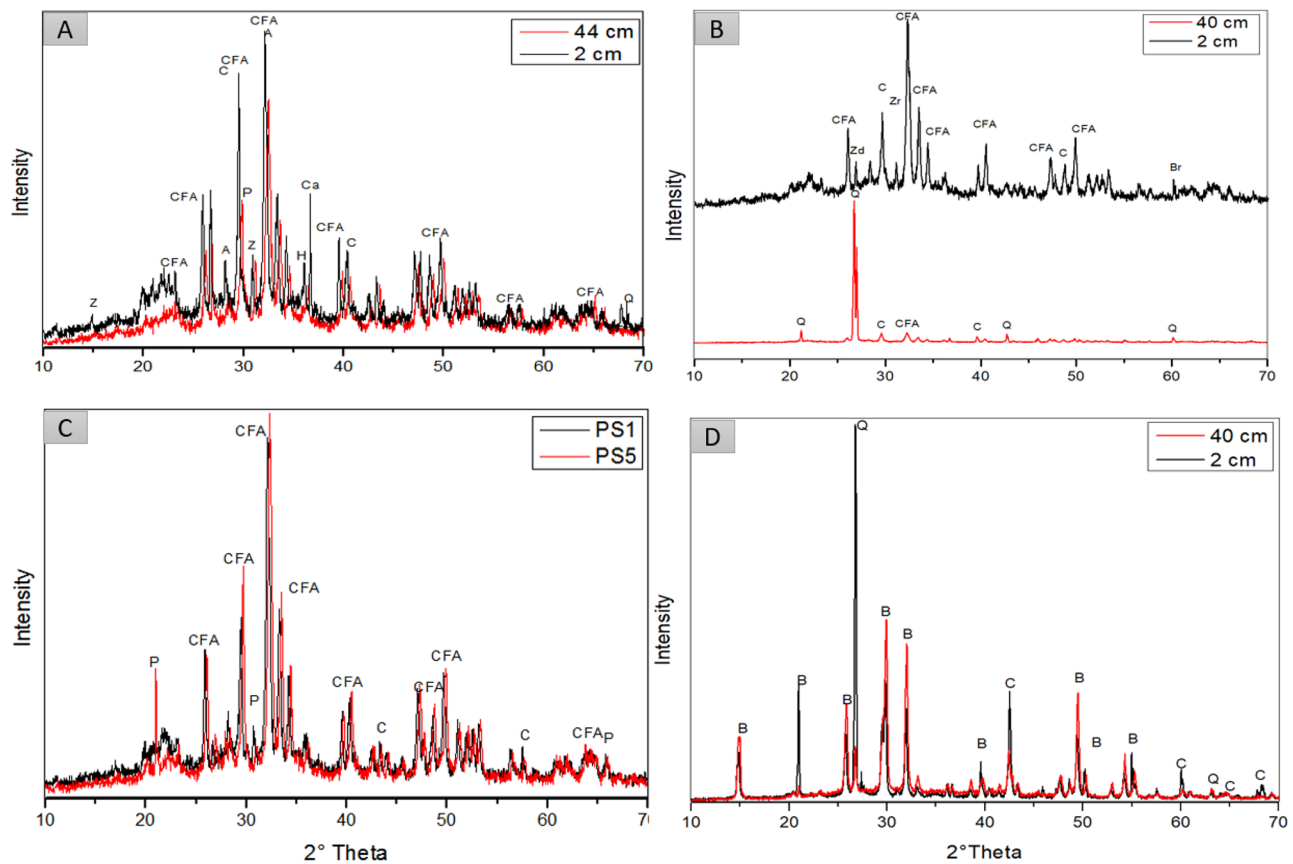


Fig. 2 XRD diffractograms of sediment profile P2 sampled at different depths of Sebseb stream in Metlaoui region (A), tailing profile P3 (B). Phosphate ore samples (C), soil samples (D). CFA: CarbonateFluor

Apatite; C: Carbonates; P: Peroskovite; B: Bassanite; Q: Quartz; Z: Zeolite; A: apatite; H: Hiortdahlyte

reported that hiortdahlyte is formed mainly in alkaline environments rich with Ca and F (Robles et al. 2001). On the other hand, peroskovite was not reported in previous research on Tunisian phosphates; however, it was stated by Rentería-Villalobos et al. (2010) that peroskovite was found in Spanish phosphates and phosphogypsum. Meanwhile, quartz (SiO_2) and zeolite were commonly found in phosphate samples and waste materials. Mine tailing profiles showed different spectra between top (2 cm) and deep profile (40 cm) with significant presence of CFA on the surface, while the mineral composition of the deeper layer seems to be influenced by the nearby soil. Meanwhile, soil samples showed a dominance of Bassanite ($\text{CaSO}_4 \cdot 1/2 \text{H}_2\text{O}$) which could be formed due to the dehydration of gypsum under arid climate ($T \geq 40^\circ\text{C}$) (Rouahna 2019). The results are quite reasonable as the phosphate enrichment process and recuperation of the apatite from the bearing matrix using flocculants, which according to Galfati et al. (2014), were proven to be not quite efficient for the total separation. In similar sampled materials of stream sediments, occasional high metal contents were found

within coarse fractions (50–2000 μm). That was believed to be owed to the nature of sediments characterized by abundance of carbonates, best known for their sorption ability of metal ions by different fixation modes (Khelifi et al. 2020a).

These findings are in accord with the previously published data of similar samples of phosphates and ore processing wastes. The effect of the bedrock is obviously dominating the mining region.

3.3 Surface elemental composition

The survey scans of phosphate rock, tailings, stream sediments, sludge, and soil are given in Fig. 3. The graphs show the varying ratios of signals of carbon (C1s), nitrogen (N1s), oxygen (O1s), fluoride (F1s), sulfur (S2p), and phosphorus (P2p) in the studied samples. The details of deconvoluted spectra are included in the Supplementary Materials.

Results showed that the most pronounced element is oxygen (XPS region: O1s) in the form of metal carbonate with a narrow high peak spectrum for all samples. Nevertheless,

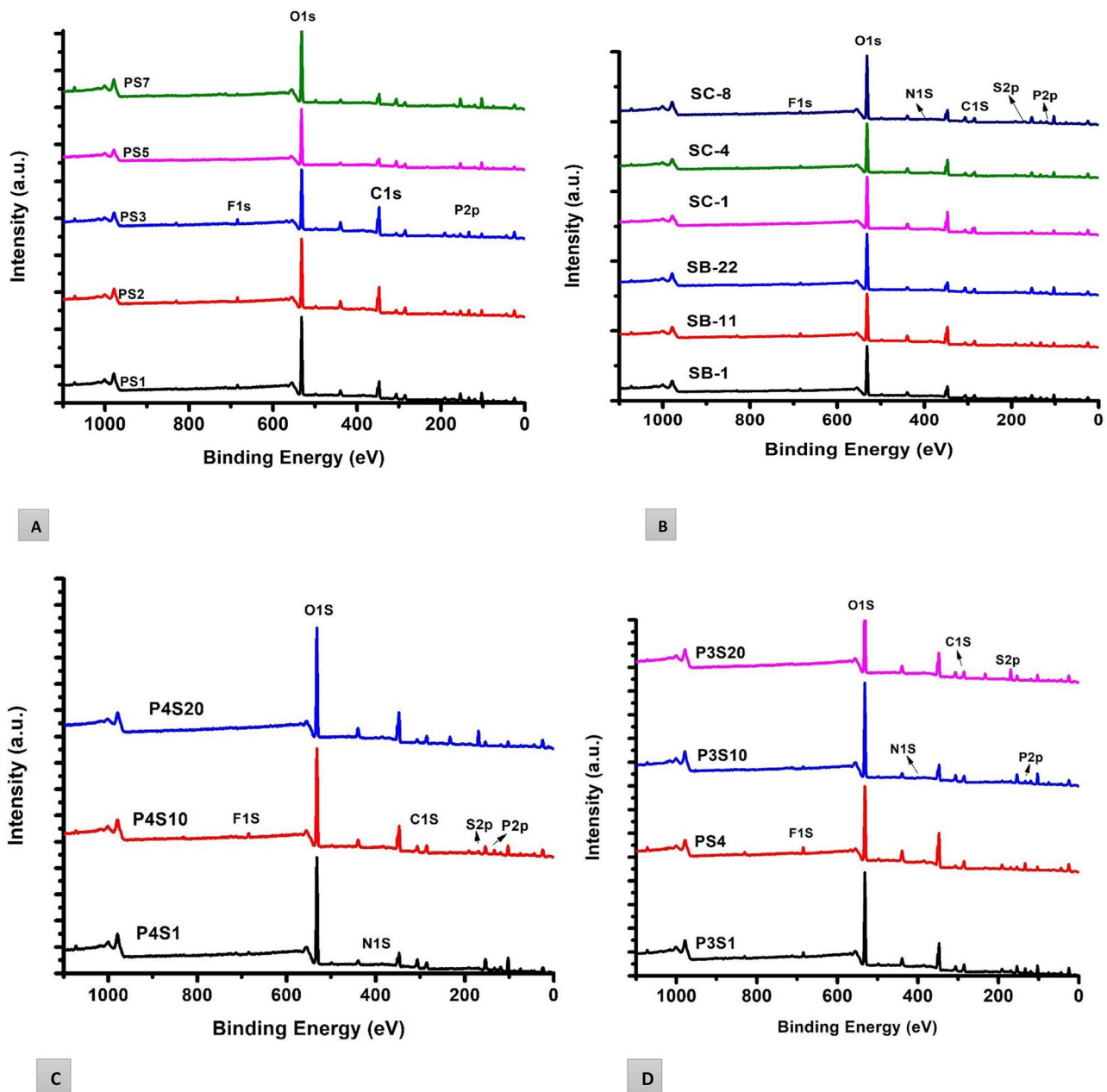


Fig. 3 XPS spectra (Survey scans) of selected samples of: (A) Phosphate ore; (B) Sediments; (C) soil; (D) tailings, collected from Gafsa-Metlaoui mining mg.kg⁻¹ showing the signals of Carbon (C1s), Nitrogen (N1s), Oxygen (O1s), Fluoride (F1s), Sulfur (S2p) and Phosphorus (P2p)

hydrous magnesium metasilicates were found in 44 cm depth and MgO in top layer (2 cm). The marked presence of oxygen in the studied samples could be related to previous exposure to the atmospheric precipitation of carbonates (Nohira et al. 2002).

At a lesser extent, the peaks of fluorine F (F1s), phosphorus P (P2p), carbon C (C1s), nitrogen N (N1s), and sulfur (S2p) are present with the corresponding chemical status: mostly zinc fluoride ZnF₂, potassium phosphate K₃PO₄,

adventitious carbon (C–C), and calcium sulfate, respectively. Furthermore, sulfates were found in the form of CaSO₄ (169.0 eV) in most of the samples (Table 2). That is most probably related to the nature of the parent materials, particularly the overlaying Jebbs (gypsum) formation. Adventitious carbon (284.8 eV) thin layer had probably formed due to an exposure of the studied materials to the atmosphere (Barr and Seal 1995).

Table 2 XPS details for main peaks of the deconvoluted spectra

Sample/subsample Depth			Chemical form					
			C1s	P2p	S2p	N1s	F1s	O1s
P	SC_1	40 cm	CdCO ₃	Ph3POBCL ₃	CaSO ₄	(NPCI ₂) ₃	ZnF ₂	As ₂ O ₅
	SC_4	20 cm	(C ₂ H ₂ O) ₃	K ₃ PO ₄	CaSO ₄	(NPCI ₂) ₃	ZnF ₂	Al ₂ O ₃ alpha
	SC_8	5 cm	(C ₂ H ₂ O) ₃	K ₃ PO ₄	CaSO ₄	Azonaphthalene	ZnF ₂	MgO
P2	SB_1	44 cm	(C ₂ H ₂ O) ₃	K ₃ PO ₄	CaSO ₄	Azonaphthalene	NaF	MgSiO ₃ ·2H ₂ O
	SB_11	22 cm	(C ₂ H ₂ O) ₃	Na ₂ HPO ₄	CaSO ₄	Ni(NH ₃) ₆ (ClO ₄) ₂	NaF	As ₂ O ₅
	SB_22	2 cm	(C ₂ H ₂ O) ₃	Ph3POBF ₃	CaSO ₄	NaN ₃	NaF	MgO
P3	P3_S1	2 cm	(C ₂ H ₂ O) ₃	K ₃ PO ₄	K ₂ SO ₄	Azonaphthalene	ZnF ₂	Al ₂ O ₃ alpha
	P3_S10	20cm	(C ₂ H ₂ O) ₃	K ₃ PO ₄	CaSO ₄	NaN ₃	NiF ₂ ·4H ₂ O	MgSiO ₃ ·2H ₂ O
	P3_S20	40 cm	(C ₂ H ₂ O) ₃	Ph3POBCL ₃	K ₂ SO ₄	Azonaphthalene	Na ₂ BeF ₄	KClO ₄
P4	P4_S1	2 cm	(C ₂ H ₂ O) ₃	K ₃ PO ₄	BaSO ₄	NaCN	NiF ₂ ·4H ₂ O	MgO
	P4_S10	20 cm	(C ₂ H ₂ O) ₃	K ₃ PO ₄	CaSO ₄	NaN ₃	ZnF ₂	Al ₂ SiO ₅
	P4_S20	40 cm	(C ₂ H ₂ O) ₃	Ph3POBF ₃	(Fe ₂ SO ₄) ₃	CH ₃ CONH ₂	NaF	MgO
PS_1	PKS	RS	(C ₂ H ₂ O) ₃	Na ₂ HPO ₄	Fe ₂ SO ₄	Ni(NH ₃) ₆ (ClO ₄) ₂	SmF ₃ /PrF ₃	CaSO ₄
PS_2			(C ₂ H ₂ O) ₃	K ₃ PO ₄	K ₂ SO ₄ /(Fe ₂ SO ₄) ₃	S ₄ N ₃ Cl	SmF ₃ /PrF ₃	Ni/Al ₂ O ₃
PS_3			(C ₂ H ₂ O) ₃	K ₃ PO ₄	CaSO ₄	S ₄ N ₃ Cl	NaF	Cr ₂ O ₃
PS_4		0–5	(C ₂ H ₂ O) ₃	K ₃ PO ₄	(Fe ₂ SO ₄) ₃	NaN ₃	ZnF ₂	As ₂ O ₅
PS_5	PKD	RS	(C ₂ H ₂ O) ₃	K ₃ PO ₄	(Fe ₂ SO ₄) ₃ /CuSO ₄	NaN ₃	ZnF ₂ /ZrF ₄	MgO
PS_6			(C ₂ H ₂ O) ₃	K ₃ PO ₄	BaSO ₄ /Al ₂ (SO ₄) ₃	NaN ₃	NiF ₂ ·4H ₂ O	MgO
PS_7		RS	(C ₂ H ₂ O) ₃	Ph3POBF ₃	CaSO ₄	S ₄ N ₃ Cl	NiF ₂ ·4H ₂ O	MgSiO ₃ ·2H ₂ O

RS representative sample

Si2p peak (103 eV) indicates the presence of Al₂SiO₅ and mullite (Al₂SiO₅), while B1s XPS region (190.5 eV) signifies boron nitride (BN) (Biesinger 2017).

XPS scans depicted the presence of elements such as carbonate, sulfate, and phosphate compounds, nitrates, oxides, and cyanides in phosphate ore samples which is in well accordance with previous reports and findings on phosphate ore and apatite (Hidalgo-Carrillo et al. 2012). Overall, stream sediments and ore tailings collected at different depths showed similar composition with the existence of compounds from phosphate ore along with alkali and alkaline earth metals. Soil samples collected from urban area also showed similar composition to tailings and stream sediments. Considering urban set up, organic compounds were found in excess in samples collected at shallow depths. Meanwhile, sludge surface composition is mostly of phosphate, carbonate, and sulfate compounds.

3.4 Major oxides

The distribution of P₂O₅ varies among the different samples as well as along the same profile according to the depth. The highest values are registered in phosphate samples with 25.2 wt%. For the sediment profile P2, the highest value was recorded in the depth of 20–22 cm with 22.19 wt%. The tailings also showed high value of P₂O₅ with 25.03 wt% (See Table 1). The profiles of sediments P and soil P4 results

yield the lowest concentrations of P₂O₅ (< 1 wt%) which tend to increase with the depth showing a peak at 20 cm depth to decrease again at 40 cm. Na₂O, Fe₂O₃ (0.37%), K₂O (0.12%), and Al₂O₃ are found to be present in low concentration with relatively higher CO₂ contents. Similarly, MgO show low concentrations (varying from 0.75 to 4.18 wt%). As a result, for the majority of the samples, MgO and P₂O₅ increased inversely while Al₂O₃ increased proportionally with SiO₂.

Broadly, the sample oxide content demonstrated that most of the samples are enriched in P₂O₅, CaO, and SiO₂. These three major oxides were proven to be of high concentrations, as reported previously by Khelifi et al. (2019) and Garnit et al. (2017). The high % are reasonable regarding the fact that phosphatic minerals should be present in the phosphate ore as well as its wastes. Their occurrence was admitted to being associated with the phosphate deposits and the enrichment process as it was proven that phosphate samples (PS2, PS3) are more enriched in P₂O₅ than the rest of the samples. However, tailing samples seem to have high P₂O₅ which indicates that the ore enrichment procedure might not be totally effective or that top tailings were tainted by raw phosphate while being transported. The high amounts of CaO were inversely proportional to SiO₂ and proportional to P₂O₅. These results were confirmed with linear correlations of CaO vs. P₂O₅ with its positive significant linear fit (0.49) and SiO₂ vs. P₂O₅ with negative linear fit (−0.39), indicating

a common mineralogical fraction for CaO and P₂O₅. CaO is primarily derived from CFA, whereas SiO₂ seems to be occluded in different mineralogical fractions, particularly in the matrix (Fig. 4). A comparable trend was observed in the study of Garnit et al. (2017).

3.5 Abundance and distribution of REE

Table 3 illustrates the distribution of REE within the different samples. The total concentrations of REE follow the abundance order La > Ce > Nd > Y > Gd > Eu > Sm > Yb > Tb. The samples showed an enrichment of light REE (LREE) over heavy REE (HREE) which were also observed in other phosphate wastes around the world (e.g., Pyrgaki et al. 2021). Comparing the results of REE of the different samples, they were found in high concentration within the sludge sample especially for Ce (406 mg kg⁻¹) surpassing by the values of PAAS. Based on average concentrations within each set of samples (soil, phosphates, and its solid effluent), the same sample showed the highest amounts of Gd, La, Nd, Sm, and Yb. Conversely to other studied profiles, Eu seems to be the most pronounced REE among the sediment profile P. Whereas all REE followed a trend within stream sediments indicating higher contents within deep layers (40 to 44 cm) compared to top sediments (2 to 4 cm) as shown in Fig. 5. Two peaks were observed for the profiles of sediments P2 and tailings P3 below 32 cm for P2, while they were registered below 15 cm for P3. The sediment profile P did not exhibit a detectable pattern for all REE; however, important peaks were noticed beneath 20 cm of depth. While

REE within the soil profile P4 showed slight peaks below 20 cm except for Nd that indicated intense peaks.

Generally, the vertical distribution of REE can be controlled by several geochemical processes (Mihajlovic et al. 2014). Considering the current state of the art, a similar trend was observed in the study of Liu et al. (2019) which was attributed, mainly, to a downward leaching of trace elements. While Zhou et al. (2014) accredited element contents toward deeper layer to the flood plain sedimentation process which preserve subsurface layers relatively undisturbed. Thus, those layers reflect the actual geochemical composition.

Conversely, phosphate samples yield lower amounts of REE. Among phosphate samples only PS5 showed high levels of Ce, Gd, La, Nd, Sm, Yb, and Y which reached 124 mg kg⁻¹. Overall, in most samples, Eu and Tb concentrations were higher than the standards.

The PAAS-normalized of analyzed REE (Fig. 6) depicts an evident enrichment of Eu and a relative abundance of Tb in most of the samples (sediments and tailings). Meanwhile, the remaining REE, particularly Y, showed a depletion tendency. The described trend was reversed for other samples which were found enriched with all REE with a slight lower abundance of Eu and Tb and a relatively high abundance of Y. The abundance of REE in sludge sample is marked by their enrichment with respect to PAAS. The enrichment-depletion trend in these samples is probably controlled by the anthropogenic activity of phosphate ore processing. A similar trend has already been demonstrated in the study by Boumaza et al. (2021) for some trace elements.

3.6 REE anomalies as proxies to track rock source

According to German et al. (1991), the most part of the studied phosphates samples were considered records for well-oxygenated shallow marine conditions which was translated to negative Ce anomalies with a value of (La/Sm)_N > 0.35. For all samples the ratio (La/Sm)_N was higher than 0.35 which implicated that the results of Ce anomalies are most likely reliable for reconstructing paleo environment and redox conditions (Morad and Felitsyn 2001).

As illustrated in Table 3, most samples showed negative Ce anomalies. Ce_{an} for phosphate samples of Kef Echfair area ranged between -1.34 and -0.44. To the contrary, samples of Kef Eddour (northern sector) indicated higher Ce anomalies (between 0.75 and 1.87) which reflects oxic depositional conditions in the southern area compared to the reduced conditions of the northern area (Wright et al. 1987). Furthermore, it is common to record precise anoxic diagenesis in similar depositional environments (Ben Hassen et al. 2010), which might be the main cause of the variation of Ce anomalies (Ce_{an}) among the studied samples or in this case a potential contamination of the samples in question. That being said, it is more likely for Ce to be in the form of,

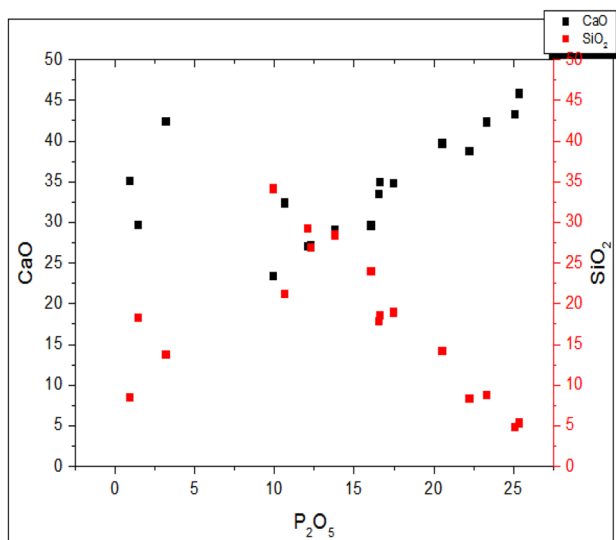


Fig. 4 Scatter plot of CaO and SiO₂ vs. P₂O₅ correlations (expressed in wt %) for phosphate, stream sediments, tailings, sludge, and soil samples of Gafsa-Metlaoui basin ($n = 19$)

Table 3 Results of REE distribution (mg kg^{-1}) in different materials and calculated anomalies

	Sediments										Phosphates										Sludge			Tailings			Soil		
	P2					P					PKS					PKD					P3			PS_04			P4		
	SB_22	SB_11	SB_1	SC_8	SC_4	SC_1	PS_01	PS_02	PS_03	PS_05	PS_06	PS_07	P3_SI	P3_S10	P3_S20	PS_04_P4	PS_04_P4	P4_SI	P4_S10	P4_S20									
La	19.59	19.10	173.35	13.33	13.47	16.00	12.36	15.16	12.32	369.31	87.20	368.70	326.29	73.76	18.37	11.56	21.09	25.76	3.61										
Ce	11.05	11.07	142.91	11.40	11.47	16.30	7.85	8.07	13.47	372.50	60.29	406.11	323.18	41.95	5.30	7.96	12.56	10.47	nd										
Nd	5.49	7.28	109.89	1.66	9.69	5.83	3.09	7.48	4.60	197.67	104.00	247.78	181.14	55.63	1.50	nd	3.94	29.87	3.44										
Sm	3.59	2.98	7.72	1.62	1.57	2.32	3.22	1.68	2.70	19.66	4.89	25.39	17.40	3.23	3.86	2.33	3.58	0.36	nd										
Eu	14.30	16.59	0.80	10.87	12.10	14.19	9.62	13.72	10.89	1.78	0.70	3.35	6.15	5.08	5.30	10.08	16.15	0.18	nd										
Gd	1.14	1.72	18.41	0.64	0.82	0.33	0.07	0.73	0.58	24.49	20.78	32.28	23.14	11.65	1.74	0.53	3.55	8.70	1.68										
Tb	1.04	3.77	0.41	1.23	0.92	1.76	0.03	1.81	0.71	nd	0.37	0.81	0.14	0.28	0.72	0.43	2.21	0.83	0.67										
Yb	0.33	0.25	5.14	0.07	0.27	0.15	0.17	0.26	0.11	6.51	5.33	7.80	6.28	3.37	0.30	0.18	0.41	1.78	0.05										
Y	3.36	0.55	73.63	0.94	0.21	0.21	0.33	0.39	0.73	124.03	53.99	145.27	117.62	40.07	0.82	0.14	1.23	18.71	0.10										
LREE (La-Eu)	55.15	58.74	453.06	39.51	49.13	54.96	36.21	46.84	44.57	985.41	277.86	1341.95	1083.60	191.30	36.07	32.45	60.87	75.35	8.73										
HREE (Gd-Lu + Y)	4.74	4.57	79.18	2.24	1.40	2.12	0.52	2.47	1.55	130.54	59.69	153.89	124.04	43.71	1.84	0.75	3.85	21.31	0.83										
LREE/HREE	11.64	12.86	5.72	17.68	35.21	25.98	69.12	18.98	28.76	7.55	4.65	8.72	8.74	4.38	19.59	43.45	15.80	3.54	10.54										
∑ REE	59.89	63.31	532.25	41.75	50.52	57.08	36.73	49.31	46.12	1115.95	337.55	1237.48	1001.33	235.01	37.91	33.20	64.72	96.66	9.56										
La/Nd	3.57	2.62	1.58	8.03	1.39	2.74	4.00	2.03	2.68	1.87	0.84	1.49	1.80	1.33	12.27	nd	5.35	0.86	1.05										
(La/Sm) N	0.79	0.93	3.26	1.19	1.25	1.00	0.56	1.31	0.66	2.73	2.59	2.11	2.72	3.32	0.69	0.72	0.86	10.40	nd										
(La/Yb) N	4.33	5.64	2.49	14.65	3.68	8.05	5.41	4.24	8.31	4.19	1.21	3.49	3.84	1.62	4.54	4.85	3.76	1.07	4.87										
Eu anomaly	14.03	16.14	0.32	15.35	16.53	18.82	11.53	18.74	12.89	0.56	0.28	0.91	2.00	2.68	4.75	12.79	12.61	0.12	nd										
Ce/Ce*	0.27	0.32	15.46	0.12	0.36	0.30	0.14	0.28	0.22	73.69	5.66	81.17	57.36	3.17	0.09	0.05	0.25	1.01	nd										
Ce anomaly	-0.57	-0.50	1.19	-0.91	-0.44	-0.52	-0.86	-0.55	-0.66	1.87	0.75	3.49	3.84	1.62	4.54	-1.34	3.76	1.07	nd										

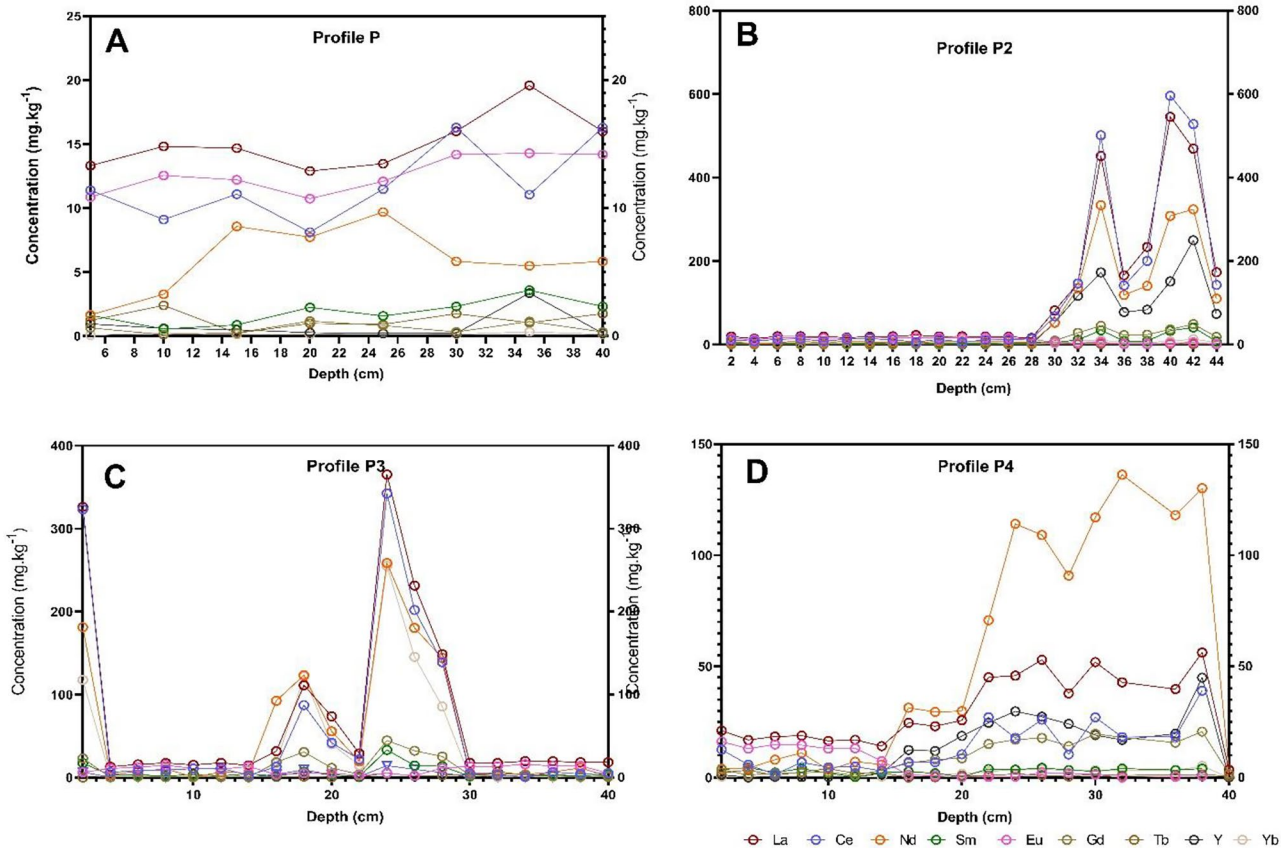
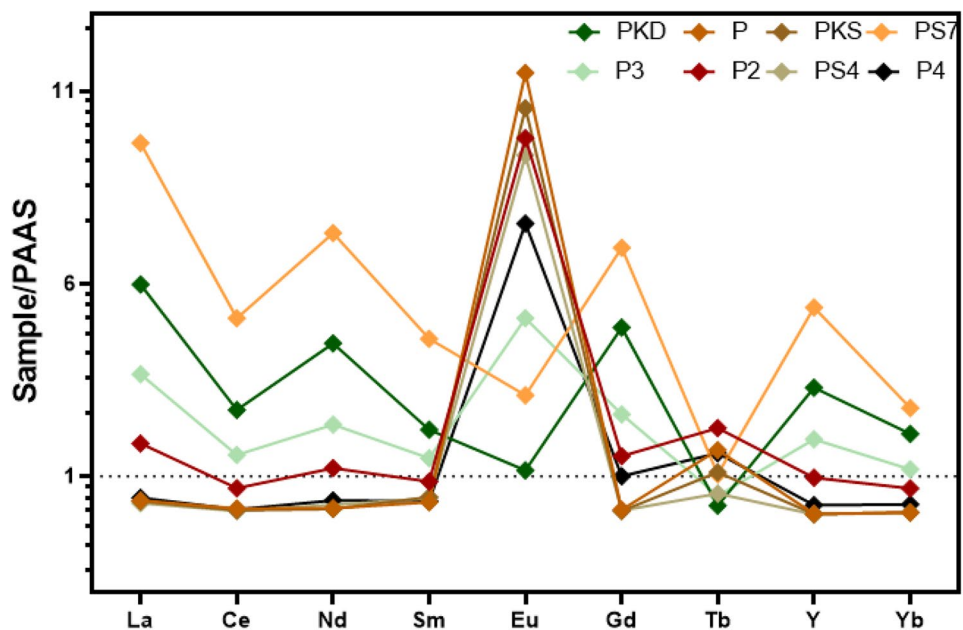


Fig. 5 Distribution of REE among different profiles: A, B stream sediment profiles, C tailing profile, and D soil profile

less soluble, Ce^{4+} in the samples of the southern area which limits its possible migration (Cao et al. 2001). Nevertheless, the Ce anomaly calculations cannot be used to reconstruct paleoenvironment and/or identify certain geochemical

patterns without considering several factors such as the early diagenesis and the late weathering effects. These factors, when not considered, could lead to obtaining an inaccurate Ce anomalies of Ce assessment.

Fig. 6 REE normalized to PAAS diagram of various sample materials: phosphate ore (PKS: PS1-3 and PKD: PS5-6), sediments (P, P2), tailings (PS4), soil (P4), and sludge (PS7) of Gafsa mining district



The previous studies conducted on representative sampling have revealed that Ce anomalies from both Tunisian and Algerian deposits are mostly suitable to track redox conditions (e.g., Garnit et al. 2017; Kechiched et al. 2020; Buccione et al. 2021; Ferhaoui et al. 2022). However, the reported values for sediments and tailing appear to be not significant due to mixing and migration of REE during enrichment process and disposal conditions.

Meanwhile, all samples showed positive Eu anomalies (Eu_{an}). Eu_{an} results of Kef Eddour sector phosphate samples (0.28 to 0.56) were found analogous to those indicated by Kechiched et al. (2020) for similar phosphate sections in Algeria. Other samples of Kef Echfair sector showed higher Eu anomalies (11.53 to 18.74), suggesting a tendency to oxic conditions in the southern area and potential warm paleo-hydrothermal conditions (Nakada et al. 2017). The results are in consistency as the lower Eu anomalies were of the same samples showing the higher positive Ce anomalies.

Lanthanum (La) anomaly showed a wide variation range (0.86 and 12.27). Generally, La anomaly is largely applied as fingerprints of methanotrophy in biological samples, e.g., shellfish mussels (Wang et al. 2020). Accordingly, the anomaly could serve for tracing the biological activity of methanotrophs responsible of aerobic methane oxidation. However, their use in geological and environmental samples is still a matter of discussion (Barrat et al. 2023).

3.7 Statistical analysis

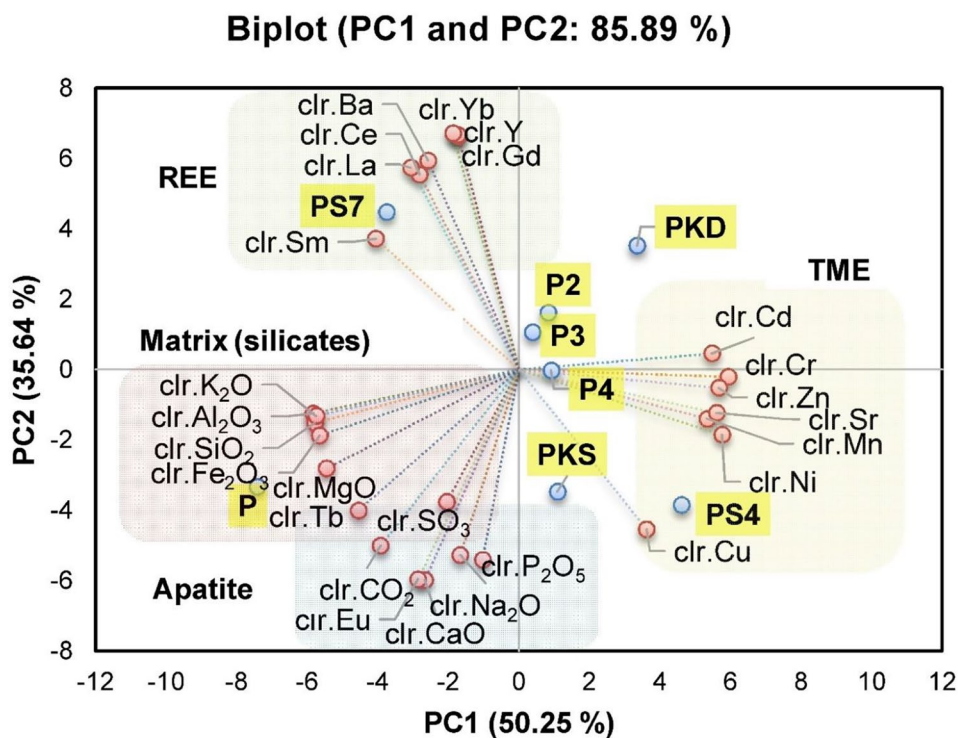
3.7.1 Pearson's correlations

Pearson's correlations were calculated on clr-data (Table S3) rather than raw data to overcome the skewed effect usually associated with geochemical data (Table S4). They show significant correlations (p -value ≤ 0.01) between clr- P_2O_5 and both clr-CaO ($r=0.87$) and clr- Na_2O ($r=0.99$), reflecting the apatite component, as stated above in the mineralogical study. The occurrence of this component in the studied samples, including sediments and soils, results from phosphate rocks that are enriched in apatite minerals (Garnit et al. 2017; Khelifi et al. 2019; Kechiched et al. 2020).

3.7.2 Principal component analysis and cluster analysis

Principal component analysis (PCA), representing one of the most common multivariate statistical treatments, was conducted using correlation matrix of clr-data (see Table S4). By reducing dimensionality, the underlined structures could be better interpreted and highlighted (Davis 1986). Here, we have much interest in depicting the main sub-compositions promoting the controls on trace metal and REE distribution in samples studied. The main components, PC1 and PC2, gather 85.89% of the total explained variance (PC1 = 50.25%, PC2 = 30.64%, PC3 = 9.55%, PC4 = 2.56%) (Table S5). Therefore, a biplot was established by plotting

Fig. 7 Biplot of the PC1 versus PC2 components from the PCA analysis on clr-transformed data



PC1 against PC2, as illustrated in Fig. 7. Within this biplot, the main trends are elucidated and interpreted.

The first trend toward a positive association with PC1 includes a group of TMEs, such as Cd, Cr, Zn, Sr, Ni, Cu, and Mn. Conversely, the subsequent trends show a negative loading with PC1, displaying three sub-trends: (1) REEs and Ba exhibit a negative loading with PC1 and a positive association with PC2, representing most of REEs (LREE: La, Ce, Sm; HREE: Gd, Y, Yb); (2) silicate and matrix elements demonstrate high negative loadings toward PC1 and low loadings on negative PC2, including K_2O , Al_2O_3 , SiO_2 , Fe_2O_3 , MgO , and Tb ; and (3) apatites exhibit high loadings toward negative PC2 and low loadings for a negative PC1, containing P_2O_5 , CaO , Na_2O , SO_3 , CO_2 , and Eu .

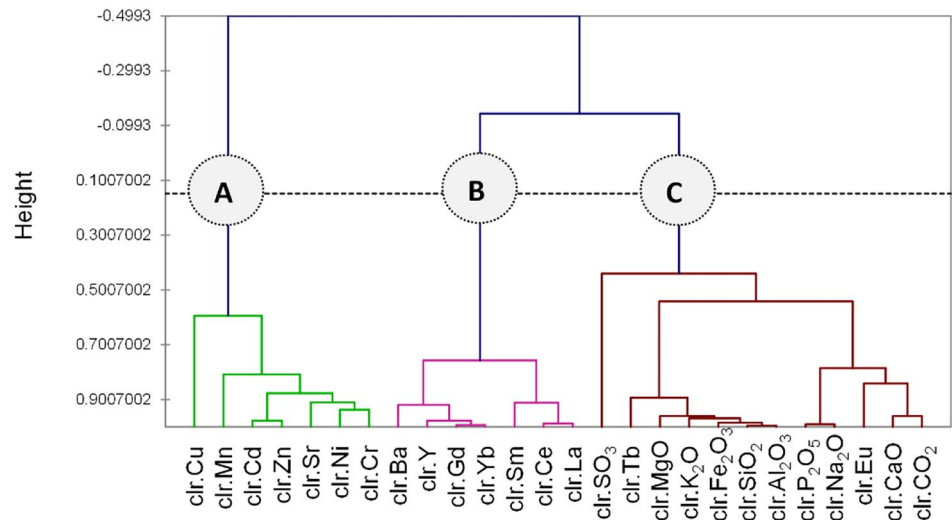
Compared to previous studies on phosphorites in Tunisia (Galfati et al. 2014; Garnit et al. 2017) and Algeria (Kechiched

et al. 2020; Boumaza et al. 2021), these trends elucidate the primary chemical components of phosphate rocks (apatites, matrix, and silicates). Additionally, it is observed that sediments and soils are influenced by mining operations.

The PCA also reveals a significant fractionation of REEs and TME among the principal mineralogical phases of the samples. The positioning of samples in the biplot indicates that some exhibit a relatively enriched composition aligned with the main trends identified by the PCA analysis. For instance, the sample PS7 is plotted on the REE zone, indicating that phosphate sludges tend to accumulate REEs during the phosphate beneficiation process, leading to the removal of REEs from phosphate and their enrichment in fine sludges. Furthermore, the sediment sample (P) shows enhancement with silicate elements, which can be attributed to the matrix component. With the exception

Fig. 8 Hierarchical cluster analysis dendrograms for the studied samples

(a): Variables



(b): Individuals

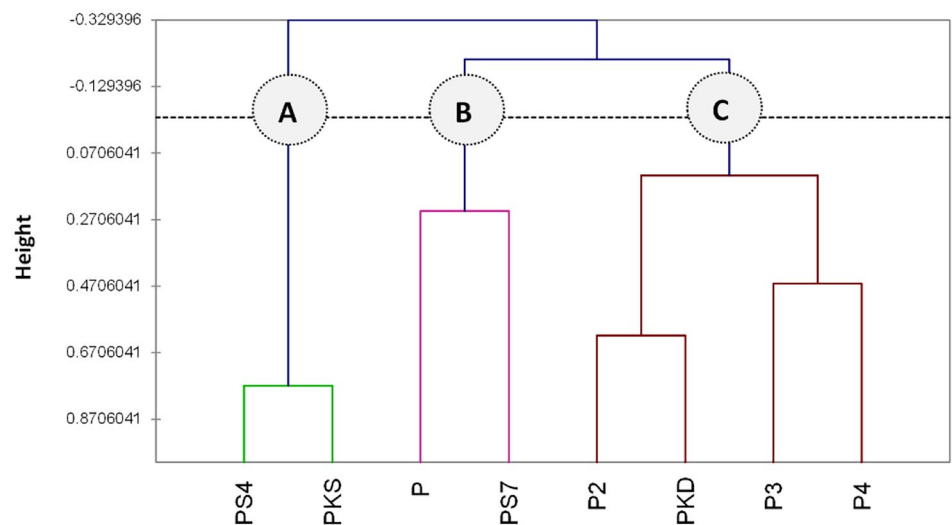


Table 4 Calculated environmental and ecological risk indices for the studied REE in phosphate samples, stream sediments, tailings, soil, and sludge

	Ce	Eu	Gd	La	Nd	Sm	Tb	Y	Yb	Σ REE
Igeo^a										
P	-3.33	2.96	-3.54	-1.92	-3.08	-2.14	0.15	-5.68	-4.52	-2.53
P2	-0.08	2.76	0.67	1.01	0.53	0.09	0.30	0.16	-0.54	0.39
P3	-0.94	2.55	0.57	0.41	0.14	-0.35	0.43	0.00	-0.55	-0.13
P4	-3.17	1.80	0.43	-0.93	0.08	-1.50	0.35	-1.60	-1.22	-1.14
PS1	-3.93	2.57	-6.55	-2.21	-4.04	-1.37	-5.33	-6.96	-4.65	-2.98
PS2	-3.89	3.08	-3.26	-1.92	-2.77	-2.31	0.64	-6.70	-4.00	-2.56
PS3	-3.15	2.75	-3.58	-2.22	-3.47	-1.62	-0.70	-5.80	-5.27	-2.65
PS4	-3.91	2.64	-3.73	-2.31	-	-1.84	-1.44	-8.14	-4.59	-3.13
PS5	1.64	0.14	1.81	2.69	1.96	1.24	-	1.61	0.62	1.94
PS6	-0.99	-1.21	1.57	0.61	1.03	-0.77	-1.65	0.41	0.33	0.22
PS7	1.77	1.05	2.21	2.69	2.28	1.61	-0.51	1.84	0.88	2.09
Igeo^b										
P	-3.02	3.26	-3.25	-1.58	-2.70	-1.84	0.43	-5.39	-4.16	-2.20
P2	0.23	3.06	0.97	1.35	0.91	0.40	0.57	0.46	-0.18	0.72
P3	-0.63	2.84	0.86	0.76	0.53	-0.05	0.70	0.30	-0.19	0.20
P4	-2.85	2.09	0.72	-0.58	0.47	-1.20	0.62	-1.30	-0.86	-0.81
PS1	-3.61	2.87	-6.25	-1.86	-3.66	-1.07	-5.05	-6.66	-4.29	-2.65
PS2	-3.57	3.38	-2.97	-1.57	-2.38	-2.00	0.92	-6.40	-3.65	-2.23
PS3	-2.83	3.04	-3.29	-1.87	-3.08	-1.32	-0.43	-5.50	-4.91	-2.32
PS4	-3.59	2.93	-3.44	-1.96	-	-1.54	-1.17	-7.84	-4.23	-2.80
PS5	1.96	0.43	2.10	3.04	2.34	1.54	-	1.91	0.98	2.27
PS6	-0.67	-0.91	1.87	0.95	1.41	-0.46	-1.38	0.71	0.69	0.55
PS7	2.08	1.34	2.50	3.03	2.67	1.91	-0.24	2.14	1.24	2.42
CF^c										
P	0.19	14.37	0.16	0.50	0.23	0.42	2.01	0.04	0.08	0.33
P2	1.76	12.49	2.93	3.84	2.81	1.97	2.23	2.06	1.33	2.48
P3	0.97	10.76	2.72	2.54	2.16	1.45	2.44	1.84	1.32	1.73
P4	0.21	6.41	2.47	1.00	2.07	0.65	2.31	0.61	0.83	0.86
PS1	0.12	10.93	0.02	0.41	0.12	0.72	0.05	0.01	0.08	0.24
PS2	0.13	15.59	0.19	0.51	0.29	0.37	2.83	0.02	0.12	0.32
PS3	0.21	12.38	0.15	0.41	0.18	0.60	1.11	0.03	0.05	0.30
PS4	0.12	11.45	0.14	0.39	-	0.52	0.67	0.01	0.08	0.22
PS5	5.82	2.03	6.44	12.31	7.60	4.37	-	5.64	2.96	7.25
PS6	0.94	0.80	5.47	2.91	4.00	1.09	0.58	2.45	2.42	2.19
PS7	6.35	3.81	8.49	12.29	9.53	5.64	1.27	6.60	3.54	8.03

Table 4 (continued)

	E ^d										RI ^e
P	0.19	143.66	0.79	0.50	0.46	2.09	20.14	0.07	0.42	168.33	
P2	1.76	124.86	14.67	3.84	5.63	9.86	22.26	4.12	6.63	193.62	
P3	0.97	107.57	13.62	2.54	4.32	7.25	24.36	3.69	6.58	170.89	
P4	0.21	64.06	12.37	1.00	4.15	3.27	23.12	1.22	4.13	113.53	
PS1	0.12	109.29	0.10	0.41	0.24	3.58	0.45	0.03	0.38	114.60	
PS2	0.13	155.91	0.96	0.51	0.58	1.87	28.34	0.04	0.60	188.93	
PS3	0.21	123.77	0.77	0.41	0.35	3.00	11.14	0.07	0.25	139.97	
PS4	0.12	114.50	0.69	0.39	–	2.58	6.67	0.01	0.40	125.37	
PS5	5.82	20.25	32.22	12.31	15.21	21.84	–	11.28	14.79	133.72	
PS6	0.94	7.97	27.34	2.91	8.00	5.44	5.77	4.91	12.12	75.39	
PS7	6.35	38.06	42.47	12.29	19.06	28.21	12.73	13.21	17.72	190.09	

^aGeoaccumulation index with respect to PAAS (post-Archean Australian shales)

^bGeoaccumulation index with respect to UCC (upper continental crust)

^cContamination factor with respect to UCC

^dSingle ecological risk

^eTotal ecological risk

of samples PKD and PS4, which are relatively enriched in some TME, the remaining samples appear to be scattered across these trends.

To further clarify these trends, the hierarchical cluster analysis (HCA) that was conducted on clr-data is presented in form of dendrograms (Fig. 8). They show visually three distinct clusters where each cluster can reflect a geochemical fingerprint.

Dendrogram mainly contains three clusters defining the main chemical associations in the studied samples. The first cluster (A) contains in trace metal elements, such as clr-Cu, clr-Mn, clr-Cd, clr-Zn, clr-Ni, and clr-Cr which are relatively enriched in PS4 and PKS samples. The second cluster (B) includes mainly rare earth and clr-Ba. This cluster fingerprints two samples (P and PS7), which represent contaminated sediments and sludge, respectively. Markedly the sludge sample (PS7) yields the maximum of \sum REEs (1237 ppm), indicating that fine fractions can therefore enhance REEs. The third cluster (C), which itself can be divided into three sub-clusters of (i) clr-SO₃; (ii) clr-Tb, clr-MgO, clr-K₂O, Fe₂O₃, Al₂O₃, SiO₂, clr-Na₂O, clr-SO₃, and clr-Al₂O₃; and (iii) clr-P₂O₅, clr-Na₂O, clr-Eu, clr-CaO, and clr-CO₂, reflecting phosphatic rock and soil patterns containing sulfates, matrix and apatite with variable amounts in the samples.

3.8 Environmental assessment and the ecological risk

The Geo-accumulation index was calculated with respect to UCC values and to PAAS values. There was no noticeable variation between the obtained results, which leaves no possibility for misinterpretation. Furthermore, there was no contamination with REE for most of the sample except for Eu that showed moderate to heavy contamination level,

reaching 3.83. Conversely, only the sludge was found moderately to heavily contaminated with REE (except for Tb).

Among the studied REE, Eu showed the highest contamination factor indicating a very high contamination level; accordingly, it reflected on the single ecological risk with a remarkable difference compared to the rest of the elements. However, it remained within < 150 threshold, signifying a low individual risk. Examining the total ecological risk (RI) of the various sampled materials reported in Table 4, values were found slightly higher than 150 with one sample that had a moderate ecological risk. However, the rest of the samples demonstrate a low ecological risk.

These results indicate that most of the samples are not contaminated with REE except for Eu. These findings indicate that the presence Eu is most probably enhanced by the phosphate processing activities. However, there is no noteworthy ecological risk associated with their enrichment.

4 Research limitations

The study faced a few limitations which consisted of providing a complete and a thorough data set particularly for REE. It is admitted that missing data could inspire an interpretative bias. Conversely, it is usually considered of insignificant role outside of the statistical framework. Generally, in the context of gathering and organizing data, it is practically inevitable to avoid missing data (Mayer et al. 2020). Examining the present results, for REE only 2.92% of the mean observations (for each profile) attributed as below detection limit (non-detected, nd). A similar case was treated in

the study of Todorović et al. (2020). While about 60% of the total REE were analyzed. Thus, the most critical REE were presented while the results of others were not provided. However, as stated in the introduction, this study is mainly intended to represent a preliminary investigation of the most abundant elements in phosphate ore, its wastes, sediments, and soil around the mining area. Therefore, for a better understanding of the geochemical patterns and fractionation, it is recommended to conduct a comprehensive analysis.

Data comparison and normalization were seen as a matter of concern as well. It is acknowledged that the concentration of REE is highly dependent on the study area and the nature of the parent rock (Li et al. 2022). However, throughout the literature, as previously mentioned in Section 2.3 due to the absence of local standards, we have used the UCC standards for index calculations. This is comparable to the recent studies conducted on sediments of China (Liu et al. 2023) and Brazil (de Freitas et al. 2021) which for that matter faced the same limitation.

While the statistical analysis was conducted after a transformation of raw data into new centered log-ratios to address issues related to linearity of data, as highlighted by several authors (e.g., Filzmoser et al. 2010), some limitations are associated with this statistical treatment, primarily due to the relatively low sample size and the mixture of data (tailing, sediments, and soils). The study has identified the fractionation of TME and REEs resulting from leaching and post-processing sedimentation of generated wastes. Therefore, future research should be undertaken to delineate the economic significance of REEs in both resources and quality based on the quantity of critical elements in the phosphate processing chain and its associated wastes and sediments.

5 Conclusions and recommendations

The study intends to evaluate the anthropogenic input of trace elements, in particular, REEs, through geochemical and mineralogical characterization of phosphate-mine-contaminated materials in a North African mining area. The main goal is achieved through several processes and revealed the following:

1. The sampled materials contain high contents of carbonate mineral mainly CAF in most of the samples.
2. Most trace elements and REEs tend to accumulate in subsurface layers (mainly below 30 cm) within sediment profile which is probably governed by the flood plain sedimentation patterns and/or potential in-depth leaching.
3. The Ce and Eu anomalies helped in reconstructing characteristics of phosphatic rock origin showing sub-oxic to oxic depositional Paleoenvironment.
4. The statistical study proved the presence of underlying similarities between the various materials. These parallels were attributed to phosphate ore processing activities and probable contamination of the surrounding environment.
5. The environmental assessment indices showed an absent contamination, a moderate enrichment of REE except for Eu which showed heavy contamination and an extreme enrichment. Y depicted a deficiency of enrichment in most of the samples except for sludge sample which was found enriched with REE as well.

In a broader context, several factors intervene with the geochemical and the mineralogical composition of stream sediments, tailing sludge, and soil of a mining area and the variation of REE within a single profile. Thus, these variations are not strictly limited to one single factor as anthropogenic activities or natural circumstances (geologic landscape, flood plain sedimentation patterns, etc.). Indeed, the examination of the studied elements highlighted the role of phosphate processing activities in enhancing the enrichment of Eu. Even though there are no proven environmental and ecological hazards associated with REE and accordingly no detrimental effects on humans associated with rare earth elements. However, the provided data could be of use in assessing the potential extraction (magnetic separation), valorization, and exploitation of such material, particularly the landfilled wastes, investing in that way in the circular economy and guaranteeing environmental sustainability.

Supplementary Information The online version contains supplementary material available at <https://doi.org/10.1007/s11368-024-03771-4>.

Acknowledgements The authors would like to thank the anonymous reviewers for their suggestions which helped in improving an earlier version of the manuscript. Analyses protocols and instrumentations were provided by the laboratories of University of Science and Technology of China and the laboratories of Hongchuang Exploration Technology Service, Nanjing-China, and supported by the Chinese Academy of Science CAS—Key Laboratory of Mantle Crust Materials and Environments (Central Universities Research fund WK2080000103).

Author contribution Conceptualization, methodology, formal analysis and investigation, writing—original draft, and writing—review and editing: F. Khelifi; methodology, writing—original draft, and writing—review and editing: S. Batool; methodology, writing—original draft, and writing—review and editing: R. Kechiched; writing—original draft and writing—review and editing: E. Padoan; writing—original draft and writing—review and editing: K. Ncibi; methodology, supervision, and writing—original draft: Y Hamed.

Funding Open access funding provided by Università degli Studi di Torino within the CRUI-CARE Agreement.

Data availability Data are included in the article and supplementary material file.

Declarations

Conflict of interest The authors declare no competing interests.

Open Access This article is licensed under a Creative Commons Attribution 4.0 International License, which permits use, sharing, adaptation, distribution and reproduction in any medium or format, as long as you give appropriate credit to the original author(s) and the source, provide a link to the Creative Commons licence, and indicate if changes were made. The images or other third party material in this article are included in the article's Creative Commons licence, unless indicated otherwise in a credit line to the material. If material is not included in the article's Creative Commons licence and your intended use is not permitted by statutory regulation or exceeds the permitted use, you will need to obtain permission directly from the copyright holder. To view a copy of this licence, visit <http://creativecommons.org/licenses/by/4.0/>.

References


- Addinsoft (2021) XLSTAT statistical and data analysis solution. New York, USA. <https://www.xlstat.com>. Accessed 4 Apr 2023
- Aitchison J (1982) The statistical analysis of compositional data. *J Royal Statist Soc Series B* 44:139–160. <https://doi.org/10.1111/j.2517-6161.1982.tb01195.x>
- Al-Hwaiti M, Brumsack H, Schnetger B (2016) Suitability assessment of phosphate mine waste water for agricultural irrigation, an example from Eshidiya mines. *South Jordan J Environ Earth Sci* 75:276. <https://doi.org/10.1007/s12665-015-4850-4>
- Ávila PF, Silva EFD, Salgueiro AR, Farinha JA (2008) Geochemistry and mineralogy of mill tailings impoundments from the Panasqueira Mine (Portugal): implications for the surrounding environment. *Mine Water Environ* 27:210–224. <https://doi.org/10.1007/s10230-008-0046-4>
- Barceló-Vidal C, Martín-Fernández JA, (2016) The mathematics of compositional analysis. *Austrian J Stat* 4:57–71. <https://doi.org/10.17713/ajs.v45i4.142>
- Barr TL, Seal S (1995) Nature of the use of adventitious carbon as a binding energy standard. *J Vac Sci Technol A* 13:1239–1246. <https://doi.org/10.1116/1.579868>
- Barrat JA, Bayon G, Lalonde S (2023) Calculation of cerium and lanthanum anomalies in geological and environmental samples. *Chem Geol* 615:121202. <https://doi.org/10.1016/j.chemgeo.2022.121202>
- Bel Haj Ali M, Jedoui Y, Dali T, Ben Salem H, Memmi L (1987) Carte géologique de la Tunisie 1: 500000. Office National des Mines. Département de la géologie, service géologique; Tunis. Tunisie. (in French)
- Ben Hassen A, Trichet J, Disnar JR, Belayouni H (2010) Pétrographie et géochimie comparées des pellets phosphatés et de leur gangue dans le gisement phosphaté de Ras-Draâ (Tunisie). Implications sur la genèse des pellets phosphatés. *Swiss J Geosci* 103:457–473. <https://doi.org/10.1007/s00015-010-0029-x>
- Biesinger MC (2017) Advanced analysis of copper X-ray photoelectron spectra. *Surf Interface Anal* 49:1325–1334. <https://doi.org/10.1002/sia.623>
- Blake S, Henry T, Murray J, Flood R, Muller MR, Jones AG, Rath V (2016) Compositional multivariate statistical analysis of thermal groundwater provenance: a hydrogeochemical case study from Ireland. *Appl Geochem* 75:171–188. <https://doi.org/10.1016/j.apgeochem.2016.05.008>
- Boumaza B, Kechiched R, Chekushina TV (2021) Trace metal elements in phosphate rock wastes from the Djebel Onk mining area (Tébessa, eastern Algeria): a geochemical study and environmental implications. *Appl Geochem* 127:104910. <https://doi.org/10.1016/j.apgeochem.2021.104910>
- Buccianti A, Nisi B, Martín-Fernandez JA, Palarea-Albaladejo J (2014) Methods to investigate the geochemistry of groundwaters with values for nitrogen compounds below the detection limit. *J Geochem Explor* 141:78–88. <https://doi.org/10.1016/j.gexplo.2014.01.014>
- Buccione R, Kechiched R, Mongelli G, Sinisi R (2021) REEs in the north Africa P-bearing deposits, paleoenvironments, and economic perspectives: a review. *Minerals* 11:214. <https://doi.org/10.3390/min11020214>
- Cao X, Chen Y, Wang X, Deng X (2001) Effects of redox potential and pH value on the release of rare earth elements from soil. *Chemosphere* 44:655–661. [https://doi.org/10.1016/S0045-6535\(00\)00492-6](https://doi.org/10.1016/S0045-6535(00)00492-6)
- Comas-Cufí M, Thió-Henestrosa S (2011) CoDaPack 2.0: a stand-alone, multi-platform compositional software. Proceedings of The 4th International Workshop on Compositional Data Analysis. <https://dugidoc.udg.edu/handle/10256/13645>. Accessed 4 Apr 2023
- Creac'h L, Noble TL, Chase Z, Charlier BL, Townsend AT, Perez-Tribouillier H, Dietz C (2023) Unradiogenic reactive phase controls the ϵNd of authigenic phosphates in East Antarctic margin sediment. *Geochim Cosmochim Acta* 344:190–206. <https://doi.org/10.1016/j.gca.2023.01.001>
- Davis JC (1986) Statistics and data analysis in geology. John Wiley & Sons Inc, New York
- de Freitas TOP, Pedreira RMA, Hatje V (2021) Distribution and fractionation of rare earth elements in sediments and mangrove soil profiles across an estuarine gradient. *Chemosphere* 264:128431. <https://doi.org/10.1016/j.chemosphere.2020.128431>
- El Ayachi MS, Zagarni MF, Snoussi A, Bahrouni N, Gzam M, Ben Assi I, Hammami K, Abdelli H, Ben Rhaïem H (2016) The Paleocene-Lower Eocene series of the Gafsa basin (South-Central Tunisia): integrated stratigraphy and paleoenvironments. *Arab J Geosci* 9:1–14. <https://doi.org/10.1007/s12517-016-2403-0>
- El Zrelli R, Baliteau JY, Yacoubi L, Castet S, Grégoire M, Fabre S, Sarazin V, Daconceicao L, Courjault-Radé P, Rabauoui L (2021) Rare earth elements characterization associated to the phosphate fertilizer plants of Gabes (Tunisia, Central Mediterranean Sea): geochemical properties and behavior, related economic losses, and potential hazards. *Sci Total Environ* 791:148268. <https://doi.org/10.1016/j.scitotenv.2021.148268>
- Emsbo P, McLaughlin PI, Breit GN, Du Bray EA, Koenig AE (2015) Rare earth elements in sedimentary phosphate deposits: solution to the global REE crisis? *Gondwana Res* 27:776–785. <https://doi.org/10.1016/j.gr.2014.10.008>
- Eskanlou A, Huang Q (2021) Phosphatic waste clay: Origin, composition, physicochemical properties, challenges, values and possible remedies – a review. *Miner Eng* 162:106745. <https://doi.org/10.1016/j.mineng.2020.106745>
- Eusden JD, Gallagher L, Eighmy TT, Crannell BS, Krzanowski JR, Butler LG, Cartledge FK, Emery EF, Shaw EL, Francis CA (2002) Petrographic and spectroscopic characterization of phosphate-stabilized mine tailings from Leadville, Colorado. *Waste Manage* 22:117–135. [https://doi.org/10.1016/S0956-053X\(01\)00060-5](https://doi.org/10.1016/S0956-053X(01)00060-5)
- Ferhaoui S, Kechiched R, Bruguier O, Sinisi R, Kocsis L, Mongelli G, Bosch D, Ameur-Zaimeche O, Laour R (2022) Rare earth elements plus yttrium (REY) in phosphorites from the Tébessa region (Eastern Algeria): abundance, geochemical distribution through grain size fractions, and economic significance. *J*

- Geochem Explor 241:107058. <https://doi.org/10.1016/j.gexplo.2022.107058>
- Filzmoser P, Hron K, Reimann C (2010) The bivariate statistical analysis of environmental (compositional) data. *Sci Total Environ* 408:4230–4238. <https://doi.org/10.1016/j.scitotenv.2010.05.011>
- Galfati I, Bilal E, Abdallah H, Beji-Sassi A (2014) Geochemistry of solid effluents and phosphate ore washed from Metlaoui-Gafsa basin, Tunisia. *Rom J Miner Depos* 87:83–86
- Garnit H, Bouhlef S, Jarvis I (2017) Geochemistry and depositional environments of Paleocene-Eocene phosphorites: Metlaoui Group, Tunisia. *J Afr Earth Sci* 134:704–736. <https://doi.org/10.1016/j.jafrearsci.2017.07.021>
- German CR, Holliday BP, Henry E (1991) Redox cycling of rare earth elements in the suboxic zone of the Black Sea. *Geochim Cosmochim Acta* 55:3553–3558. [https://doi.org/10.1016/0016-7037\(91\)90055-A](https://doi.org/10.1016/0016-7037(91)90055-A)
- Greczynski G, Hultman L (2020) Compromising science by ignorant instrument calibration - need to revisit half a century of published XPS data. *Angew Chem Int Ed Engl* 59:5002–5006. <https://doi.org/10.1002/ange.201916000>
- Håkanson L (1980) An ecological risk index for aquatic pollution control. A Sedimentological Approach *Water Res* 14:975–1001. [https://doi.org/10.1016/0043-1354\(80\)90143-8](https://doi.org/10.1016/0043-1354(80)90143-8)
- Hamed Y (2013) The hydrogeochemical characterization of groundwater in Gafsa- Sidi Boubaker region (Southwestern Tunisia). *Arab J Geosci* 6:697–710. <https://doi.org/10.1007/s12517-011-0393-5>
- Hamed Y, Khelifi F, Houda B, Ben Saad A, Ncibi K, Hadji R, Melki A, Hamad A (2022) Phosphate mining pollution in southern Tunisia: environmental, epidemiological, and socioeconomic investigation. *Environ Dev Sustain* 25:13619–13636. <https://doi.org/10.1007/s10668-022-02606-x>
- Hidalgo-Carrillo J, Sebti J, Marinas A, Marinas JM, Sebti S, Urbano FJ (2012) XPS evidence for structure-performance relationship in selective hydrogenation of crotonaldehyde to crotyl alcohol on platinum systems supported on natural phosphates. *J Colloid Interface Sci* 382:67–73. <https://doi.org/10.1016/j.jcis.2012.05.050>
- Kechiched R, Laouar R, Bruguier O, Salmi-Laouar S, Kocsis L, Bosch D, Foufou A, Ameur-Zaimeche O, Larit H (2018) Glauconite-bearing sedimentary phosphorites from the Tébessa region (eastern Algeria): evidence of REE enrichment and geochemical constraints on their origin. *J Afr Earth Sci* 145:190–200. <https://doi.org/10.1016/j.jafrearsci.2018.05.018>
- Kechiched R, Laouar R, Bruguier O, Kocsis L, Salmi-Laouar S, Bosch D, Ameur Zaimeche O, Fougou A, Larit H (2020) Comprehensive REE+Y and sensitive redox trace elements of Algerian phosphorites (Tebessa, eastern Algeria): a geochemical study and depositional environments tracking. *J Geochem Explor* 208:106396. <https://doi.org/10.1016/j.gexplo.2019.106396>
- Khelifaoui M, Medjram MS, Kabir A, Zouied D, Mehri K, Chikha O, Ayadi Trabelsi M (2020) Chemical and mineralogical characterization of weathering products in mine wastes, soil, and sediment from the abandoned Pb/Zn mine in Skikda, Algeria. *Environ Earth Sci* 79:1–15. <https://doi.org/10.1007/s12665-020-09043-x>
- Khelifi F, Besser H, Ayadi Y, Liu G, Yousaf B, Harabi S, Bedoui S, Zighmi K, Hamed Y (2019). Evaluation of potentially toxic elements' (PTEs) vertical distribution in sediments of Gafsa–Metlaoui mining basin (Southwestern Tunisia) using geochemical and multivariate statistical analysis approaches. *Environ Earth Sci*. <https://doi.org/10.1007/s12665-019-8048-z>
- Khelifi F, Caporale AG, Hamed Y, Adamo P (2020a) Bioaccessibility of potentially toxic metals in soil, sediments and tailings from a north Africa phosphate-mining area: insight into human health risk assessment. *J Environ Manage* 279:111634. <https://doi.org/10.1016/j.jenvman.2020.111634>
- Khelifi F, Melki A, Hamed Y, Adamo P, Caporale AG (2020b) Environmental and human health risk assessment of potentially toxic elements in soil, sediments, and ore processing wastes from a mining area of southwestern Tunisia. *Environ Geochem Health* 42:4125–4139. <https://doi.org/10.1007/s10653-019-00434-z>
- Khelifi F, Mokadem N, Liu G, Yousaf B, Zhou H, Ncibi K, Hamed Y (2021) Occurrence, contamination evaluation and health risks of trace metals within soil, sediments and tailings in southern Tunisia. *Int J Environ Sci Technol*. <https://doi.org/10.1007/s13762-021-03531-8>
- Kocsis L, Ounis A, Baumgartner C, Pirkenseer C, Harding IC, Adatte T, Chabaani F, Neili SM (2014) Paleocene-Eocene palaeoenvironmental conditions of the main phosphorite deposits (Chouabine Formation) in the Gafsa Basin, Tunisia. *J African Earth Sci* 100:586–597. <https://doi.org/10.1016/j.jafrearsci.2014.07.024>
- Li WS, Zuo YP, Wang LQ, Wan X, Yang J, Liang T, Song H, Weihrach C, Rinklebe J (2022) Abundance, spatial variation, and sources of rare earth elements in soils around ion-adsorbed rare earth mining areas. *Environ Pollut* 313:120099. <https://doi.org/10.1016/j.envpol.2022.120099>
- Liu WS, Guo MN, Liu C, Yuan M, Chen XT, Huot H, Zhao CM, Tang YT, Morel JL, Qiu RL (2019) Water, sediment, and agricultural soil contamination from an ion adsorption rare earth mining area. *Chemosphere* 216:75–83. <https://doi.org/10.1016/j.chemosphere.2018.10.109>
- Liu Z, Gu X, Lian M, Wang J, Xin M, Wang B, Ouyang W, He M, Liu X, Lin C (2023) Occurrence, geochemical characteristics, enrichment, and ecological risks of rare earth elements in sediments of “the Yellow river–estuary–bay” system. *Environ Pollut* 319:121025. <https://doi.org/10.1016/j.envpol.2023.121025>
- Mayer I, Sverdrup E, Gauss T, Moyer JD, Wager S, Josse J (2020) Doubly robust treatment effect estimation with missing attributes. *Ann Appl Statist* 14:1409–1431. <https://doi.org/10.1214/20-aos1356>
- Mihajlovic J, Giani L, Stärk HJ et al (2014) Concentrations and geochemical fractions of rare earth elements in two different marsh soil profiles at the North Sea, Germany. *J Soils Sediments* 14:1417–1433. <https://doi.org/10.1007/s11368-014-0895-3>
- Moulder JF, Stickle WF, Sobol PE, Bomben KD (1992) Handbook of X-ray photoelectron spectroscopy. Eden Prairie, USA: Perkin-Elmer Corporation
- Morad S, Felitsyn S (2001) Identification of primary Ce-anomaly signatures in fossil biogenic apatite: implication for the Cambrian oceanic anoxia and phosphogenesis. *Sediment Geol* 143:259–264. [https://doi.org/10.1016/S0037-0738\(01\)00093-8](https://doi.org/10.1016/S0037-0738(01)00093-8)
- Müller G (1969) Index of geoaccumulation in the sediments of the Rhine River. *Geol J* 2:108–118
- Nakada R, Shibuya T, Suzuki K, Takahashi Y (2017) Europium anomaly variation under low-temperature water-rock interaction: a new thermometer. *Geochem Int* 55:822–832. <https://doi.org/10.1134/S001670291709004X>
- Nelson DW and Sommer LE (1982) Total carbon, organic carbon and organic matter. methods of soil analysis, part 2. Chemical and microbiological properties, 2nd Edition. ASA-SSSA, Madison, 595–579
- Nohira H, Tsai W, Besling W, Young E et al (2002) Characterization of ALCVD- Al_2O_3 and ZrO_2 layer using X-ray photoelectron spectroscopy. *J Non Cryst Solids* 303:83–87. [https://doi.org/10.1016/S0022-3093\(02\)00970-5](https://doi.org/10.1016/S0022-3093(02)00970-5)
- Ounis A, Kocsis L, Chaabani F, Pfeifer HR (2008) Rare earth elements and stable isotope geochemistry ($\delta^{13}C$ and $\delta^{18}O$) of phosphorite deposits in the Gafsa Basin, Tunisia. *Palaeogeogr Palaeoclimatol Palaeoecol* 268:1–18. <https://doi.org/10.1016/j.palaeo.2008.07.005>
- Padoan E, Hernandez Kath A, Vahl LC, Ajmone-Marsan F (2020) Potential release of zinc and cadmium from mine-affected soils under flooding, a mesocosm study. *Arch Environ Contam Toxicol* 79:421–434. <https://doi.org/10.1007/s00244-020-00777-0>

- Palarea-Albaladejo J, Martín-Fernández JA, Buccianti A (2014) Compositional methods for estimating elemental concentrations below the limit of detection in practice using R. *J Geochem Explor* 141:71–77. <https://doi.org/10.1016/j.gexplo.2013.09.003>
- Pawłowsky-Glahn V, Egozcue JJ, Tolosana-Delgado R (2015) Modeling and analysis of compositional data. John Wiley & Sons Ltd, Chichester
- Pyrgaki K, Gemeni V, Karkalis C, Koukouzas N, Koutsovitis P, Petrounias P (2021) Geochemical occurrence of rare earth elements in mining waste and mine water: a review. *Minerals* 11:860. <https://doi.org/10.3390/min11080860>
- Reimann C, Filzmoser P, Garrett RG, Dutterl R (2008) Statistical data analysis explained: applied environmental statistics with R. John Wiley & Sons Ltd, Chichester
- Rentería-Villalobos M, Vioque I, Mantero J, Manjón G (2010) Radiological, chemical, and morphological characterizations of phosphate rock and phosphogypsum from phosphoric acid factories in SW Spain. *J Hazard Mater* 181:193–203. <https://doi.org/10.1016/j.jhazmat.2010.04.116>
- Robles ER, Fontan F, Monchoux P, Sørensen HO, Parseval P (2001) Hiortdahlite II from the Ilímaussaq alkaline complex, South Greenland, the Tamazeght complex, Morocco, and the Iles de Los, Guinea. *Geology Greenland Surv Bull* 190:131–137. <https://doi.org/10.34194/ggub.v190.5183>
- Rouahna (2019) Individualisation de gypse dans les sols de la plaine de l'Outaya. Thèse en Sciences agronomiques. Université Mohamed Kheider Biskra Algeria. <http://thesis.univbiskra.dz/4519/1/these%20rouahna%202019%20pdf.pdf>. Accessed 5 Aug 2023
- Shields G, Stille P (2001) Diagenetic constraints on the use of cerium anomalies as palaeoseawater redox proxies: an isotopic and REE study of Cambrian phosphorites. *Chem Geol* 175:29–48. [https://doi.org/10.1016/S0009-2541\(00\)00362-4](https://doi.org/10.1016/S0009-2541(00)00362-4)
- Taha Y, Elghali A, Hakkou R, Benzaazoua M (2021) Towards zero solid waste in the sedimentary phosphate industry: challenges and opportunities. *Minerals* 11:1250. <https://doi.org/10.3390/min1111250>
- Todorović M, Čuk Đurović M, Štrbački J, Papić P (2020) Rare earth elements in mineral waters in Serbia. *Environ Earth Sci* 79:1–12. <https://doi.org/10.1007/s12665-020-09029-9>
- Wang X, Barrat JA, Bayon G, Chauvaud L, Feng D (2020) Lanthanum anomalies as fingerprints of methanotrophy. *Geochem Persp Lett* 14:26–30. <https://doi.org/10.7185/geochemlet.2019>
- Wright J, Schrader H, Holser WT (1987) Paleoredox variations in ancient oceans recorded by rare earth elements in fossil apatite. *Geochim Cosmochim Acta* 51:631–644. [https://doi.org/10.1016/0016-7037\(87\)90075-5](https://doi.org/10.1016/0016-7037(87)90075-5)
- Wu J, Lu J, Li LM, Min XY, Zhang ZH, Luo YM (2018) Distribution, pollution, and ecological risks of rare earth elements in soil of the northeastern Qinghai-Tibet plateau. *Hum Ecol Risk Assess* 25:1–16. <https://doi.org/10.1080/10807039.2018.1475215>
- Xin H, Jiang S, Yang J, Wu H, Pi D (2016) Rare earth element geochemistry of phosphatic rocks in Neoproterozoic Ediacaran Doushantuo Formation in Hushan Section from the Yangtze Gorges Area, South China. *J Earth Sci* 27:204–210. <https://doi.org/10.1007/s12583-015-0653-5>
- Yang H, Zhao Z, Fan H, Zeng M, Xiao J, Liu X, Wu S, Chao J, Xia Y (2024) Fe-(oxyhydr)oxide participation in REE enrichment in early Cambrian phosphorites from South China: evidence from in-situ geochemical analysis. *J Asian Earth Sci*. <https://doi.org/10.1016/j.jseaes.2023.105910>
- Zarasvandi A, Fereydouni Z, Alizadeh B, Absar N, Dutt Shukla A, Qaim Raza M, Ashok M, Zentilli M (2021) Phosphogenesis in the zagros fold-thrust belt, Iran: the link between the tethyan paleoenvironment and phosphate ore deposition. *Ore Geol Rev* 139:104563. <https://doi.org/10.1016/j.oregeorev.2021.104563>
- Zhou G, Sun B, Zeng D, Wei H, Liu Z, Zhang B (2014) Vertical distribution of trace elements in the sediment cores from major rivers in east China and its implication on geochemical background and anthropogenic effects. *J Geochem Explor* 139:53–67. <https://doi.org/10.1016/j.gexplo.2013.03.007>

Publisher's Note Springer Nature remains neutral with regard to jurisdictional claims in published maps and institutional affiliations.

Authors and Affiliations

Faten Khelifi¹  · Sadia Batool² · Rabah Kechiched³ · Elio Padoan¹ · Kaouther Ncibi⁴ · Younes Hamed⁴

✉ Faten Khelifi
faten.khelifi@unito.it

Sadia Batool
sbchem@f.rwu.edu.pk

Rabah Kechiched
kechiched.rabah@univ-ouargla.dz

Elio Padoan
elio.padoan@unito.it

Kaouther Ncibi
nkawther@yahoo.fr

Younes Hamed
hamed_younes@yahoo.fr

¹ Department of Agricultural, Forest and Food Sciences (DISAFA), University of Torino, Grugliasco, TO, Italy

² Department of Chemistry, Rawalpindi Women University, 6th Road, Satellite Town, Rawalpindi 9 46000, Pakistan

³ Laboratoire des Réservoirs Souterrains, Pétroliers, Gaziers et Aquifères, Université Kasdi Merbah Ouargla, Ouargla 30000, Algeria

⁴ Laboratory of Application of Materials to the Environment, Water and Energy (LAMEEE), University of Gafsa, City Campus Sidi Ahmed Zarroug, 2112 Gafsa, Tunisia